© 2023. Published by The Company of Biologists Ltd | Journal of Cell Science (2023) 136, jcs260554. doi:10.1242/jcs.260554

RESEARCH ARTICLE

Lsp1 partially substitutes for Pil1 function in eisosome assembly under stress conditions

Petra Vesela, Jakub Zahumensky and Jan Malinsky*

ABSTRACT

Eisosomes are large hemitubular structures that underlie the invaginated microdomains in the plasma membrane of various ascomycetous fungi, lichens and unicellular algae. In fungi, they are organized by BAR-domain containing proteins of the Pil1 family. Two such proteins, Pil1 and Lsp1, participate in eisosome formation in the yeast *Saccharomyces cerevisiae*. Under normal laboratory conditions, deletion of the *PIL1* gene results in the inability of cells to assemble wild-type-like eisosomes. We found that under certain stress conditions, Lsp1 partially substitutes for the Pil1 function and mediates assembly of eisosomes, specifically following a decrease in the activity of serine palmitoyltransferase, for example, in response to hyperosmotic stress. Besides Lsp1, the assembly of eisosomes lacking Pil1 also requires Seg1 and Nce102 proteins. Using next-generation sequencing, we found that the *seg1Δnce102Δpil1Δ* strain, which is unable to form eisosomes, overexpresses genes coding for proteins of oxidative phosphorylation and tricarboxylic acid cycle. By contrast, genes involved in DNA repair, ribosome biogenesis and cell cycle are downregulated. Our results identify Lsp1 as a stress-responsive eisosome organizer and indicate several novel functional connections between the eisosome and essential cellular processes.

KEY WORDS: Eisosome, Membrane compartment of Can1, Sphingolipid, Stress, Pil1, Lsp1

INTRODUCTION

The eisosome is a plasma membrane-associated protein complex described in numerous fungal species, whose core consists of Pil1 family proteins (Walther et al., 2006). Membrane association of Pil1-like proteins is mediated by their Bin/Amphiphysin/Rvs (BAR) domain and induces negative membrane curvature. Moreover, these proteins self-assemble when associated with membranes, leading to liposome tubulation *in vitro* and the formation of the hemitubular core of the eisosome *in vivo* (Ziółkowska et al., 2011; Karotki et al., 2011; Olivera-Couto et al., 2011; Suarez et al., 2014). Therefore, plasma membrane microdomains associated with the eisosome, known as the membrane compartments of Can1 (MCC), have a typical furrow shape (Stradalova et al., 2009).

The composition of the MCC and eisosome (hereafter MCC/eisosome) is highly variable. It changes depending on instantaneous conditions such as nutrient availability, membrane potential and membrane tension (Malínská et al., 2003; Grossmann et al., 2007; Berchtold et al., 2012; Gournas et al., 2016; Riggi et al., 2018; Malinsky and Opekarová, 2016; Zahumensky and Malinsky, 2019). The dynamic adaptability of the MCC/eisosome structure suggests that it has a role in cellular stress perception and response, and indeed, numerous stress-related phenotypes have been reported in cells defective in MCC/eisosome formation to date (Young et al., 2002; Zhang et al., 2004; Fröhlich et al., 2009; Dupont et al., 2010; Mascaraque et al., 2013). Fungi in nature are constantly facing different kinds of stress. It is, therefore, not surprising that not only the Pil1 family proteins but also other components of the MCC/eisosome have been conserved during phylogenetic evolution (Stradalova et al., 2009; Loibl et al., 2010; Moreira et al., 2012; Grousl et al., 2015; Lee et al., 2015).

Cells of many fungal species contain two homologous eisosome core proteins with slightly different biological functions. In the filamentous fungus *Aspergillus nidulans*, the two eisosomal organizers PilA and PilB form eisosomes at the spore periphery, whereas mycelial eisosomes only contain PilA (Vangelatos et al., 2010). In the fission yeast *Schizosaccharomyces pombe*, eisosomes in the spore membrane are composed exclusively of Pil2, whereas eisosomes at the plasma membrane of cells generated during the mitotic cell cycle, including the membrane of the ascus, contain only Pil1 (Kabeche et al., 2011). In the budding yeast *Saccharomyces cerevisiae*, distinct phosphorylation patterns of two Pil1 family proteins in the presence of sphingolipid precursors, long-chain bases (LCBs), formed the basis for the naming of these proteins: Pil1 – phosphorylation inhibited by LCBs, and Lsp1 – LCBs stimulate phosphorylation (Zhang et al., 2004). Under normal laboratory conditions (cultivation at 30°C in a nutrient-rich medium), Pil1 is dominant and sufficient to produce the normal eisosomal pattern in *S. cerevisiae*, which consists of several tens of evenly distributed and randomly oriented 250–300 nm long eisosomes per cell. Although no structural phenotype is observed in *lsp1Δ* cells, deletion of *PIL1* has a pronounced effect on the plasma membrane structure. Instead of regular eisosomes, rare (usually 1–2 per cell) collapsed structures containing MCC/eisosome-specific proteins including Lsp1 (eisosome remnants) that are up to 1 µm in size are formed in the plasma membrane of *pil1Δ* cells (Walther et al., 2006; Stradalova et al., 2009). The role of Lsp1 becomes apparent as the cell culture ages and consumes available nutrients. Under these conditions, eisosomes become larger and more numerous, which requires the presence of Lsp1 (Gournas et al., 2018).

The long all-trans acyl chains contained in sphingolipid molecules increase plasma membrane order (Boggs, 1987; Simons and Ikonen, 1997; Aresta-Branco et al., 2011; Vecer et al., 2014; Herman et al., 2015). Therefore, the cell increases their abundance in the membrane in situations that challenge the membrane integrity, such as increased temperature or membrane

Department of Functional Organization of Biomembranes, Institute of Experimental Medicine, Academy of Sciences of the Czech Republic, 142 20 Prague, Czech Republic.

*Author for correspondence (jan.malinsky@iem.cas.cz)

P.V., 0000-0002-3670-5841; J.Z., 0000-0002-8332-9789; J.M., 0000-0002-1433-0989

Handling Editor: Jennifer Lippincott-Schwartz
Received 22 August 2022; Accepted 22 December 2022

Journal of Cell Science (2023) 136, jcs260554. doi:10.1242/jcs.260554

tension. Eisosome assembly, which requires proteins of the Pil1 family, has also been shown to dynamically respond to these challenges (Berchtold et al., 2012). The direct involvement of Pil1-like proteins in the regulation of stress adaptation has been repeatedly reaffirmed in recent studies of cells lacking any of the Pil1-like proteins (Yang and Tavazoie, 2020; Sakata et al., 2022).

A specific role of Pil1 phosphorylation in the eisosome assembly has been confirmed (Walther et al., 2007; Luo et al., 2008). Minor participation of Lsp1 in eisosome formation in *S. cerevisiae* has been explained in terms of its reduced ability to bind the plasma membrane (Walther et al., 2006; Olivera-Couto et al., 2011). Given the aforementioned difference in LCB-dependent phosphorylation of Pil1 and Lsp1 proteins, we tested the hypothesis that Lsp1 can substitute for Pil1 function in eisosome assembly under stress conditions, especially when sphingolipid abundance in the plasma membrane is affected. We find that Lsp1 is able to form eisosomes independently of Pil1 and does so under conditions that decrease the activity of the serine palmitoyltransferase (SPT), such as upon its direct inhibition or hyperosmotic shock. We document that Lsp1 requires the presence of either the tetraspan protein Nce102 accumulated in the MCC (Grossmann et al., 2008; Vaskovicova et al., 2020) or the soluble eisosome stabilizer Seg1 (Moreira et al., 2012; Vaskovicova et al., 2015) to do so.

RESULTS

Heat and salt stress induce the formation of eisosomes in cells lacking Pil1

In the absence of Pil1, Lsp1 and other MCC/eisosome components accumulate in eisosome remnants in cells cultivated under normal conditions (Walther et al., 2006; Stradalova et al., 2009). Using fluorescently labeled Lsp1 as the compartment marker, we monitored the morphology of eisosome remnants in *pil1*Δ cells under conditions of membrane stress, induced either by shifting the exponentially growing yeast cultures from optimal 28°C to 37°C for 2 h or by the addition of 1 M NaCl to the growth medium. Both heat and salt stress conditions led to remarkable changes in the cellular distribution of Lsp1–GFP. Specifically, eisosome remnants disintegrated and multiple smaller-sized foci of high fluorescence intensity formed instead (Fig. 1A,B). These well-defined Lsp1–GFP foci were distributed almost evenly along the plasma membrane, had comparable brightness to each other and were of the same size and shape (Fig. S1A–D). Their number was lower compared to the wild-type eisosomes, but significantly higher than the number of eisosome remnants under both tested stress conditions (Fig. 1A,B). In addition, quantification of the plasma membrane/cytoplasm fluorescence intensity ratio and the mean cellular GFP intensity showed a clear increase in both parameters following cultivation in the presence of 1 M NaCl (Fig. 1C,D). These results indicate an increased association of Lsp1–GFP with the plasma membrane and an elevated level of the protein in response to salt stress, respectively. We confirmed the latter by using western blot analysis (Fig. 1E).

To determine whether the Lsp1-containing foci formed in response to heat and salt stress are eisosomes, we checked one of the main distinguishing features of these structures – their ability to bend the plasma membrane into the characteristic furrow shape. On freeze-etched replicas, we compared the plasma membrane morphology in *pil1*Δ cells under normal and stress conditions. We found that whereas only irregular, convoluted membrane-containing eisosome remnants in otherwise flat plasma membrane could be detected under normal conditions, salt stress induced the formation of typical wild-type-like linear furrow invaginations in the plasma membrane of *pil1*Δ cells (Fig. 2). Heat stress exposure likewise induced eisosome formation in the *pil1*Δ cells (data not shown). We, therefore, conclude that the Lsp1–GFP foci described above, formed in response to heat and salt stress, correspond to eisosomes.

Given that we have found an increase in *LSP1* expression in response to salt stress (Fig. 1E), we tested whether elevating the Lsp1 level is sufficient to induce the formation of Lsp1 eisosomes in *pil1*Δ cells even in the absence of stress. We increased *LSP1* expression by exchanging its native promoter for the $tetO_7$ promoter using the pCM225 cassette, resulting in a threefold increase in the mean cellular Lsp1–GFP fluorescence (Fig. S1E,G). The overexpression of *LSP1* led to increased accumulation of the protein within the eisosome remnants but did not trigger eisosome formation (Fig. S1E,F). When exposed to heat or salt stress, the *pil1*Δ cells overexpressing *LSP1* formed eisosomes, analogous to *pil1*Δ cells expressing *LSP1* from its native promoter (compare Fig. S1E,F with Fig. 1A,B). We conclude that the principle underlying the disintegration of eisosome remnants and formation of well-defined Lsp1 eisosomes in response to stress is not a change in Lsp1 protein abundance, but some other aspect of the stress response.

Lsp1 eisosome formation correlates with decreased serine palmitoyltransferase activity

It has been reported that both heat and salt stress induce changes in the sphingolipid composition of the yeast plasma membrane (Dickson et al., 1997; Jenkins et al., 1997; Manzanares-Estreder et al., 2017; Zahumenský et al., 2022). We, therefore, investigated whether specific modifications of the cellular sphingolipid content could induce the dissolution of the eisosome remnants in the *pil1*Δ strain and the formation of the Lsp1 eisosomes.

Heat stress causes a transient increase in the levels of LCBs, phytosphingosine (PHS) and dihydrosphingosine (DHS) (Dickson et al., 1997; Jenkins et al., 1997). In turn, LCB levels regulate Pkh1,2-mediated phosphorylation of Pil1 and Lsp1, which governs the eisosome assembly (Zhang et al., 2004; Walther et al., 2007; Luo et al., 2008). We, therefore, hypothesized, that the increase in LCBs in response to heat stress could be sufficient to trigger the formation of Lsp1 eisosomes in the absence of Pil1. To test this hypothesis, we supplied exponentially growing cells with exogenous PHS. As expected, the effect was comparable to that of heat stress. Specifically, eisosome remnants dissolved and Lsp1 eisosomes were formed in cells incubated with PHS (Fig. 3A,B). Consistent with this, the mean intensity and length of Lsp1–GFP patches in the plasma membrane decreased (Fig. S2).

Cultivation of the cells in the presence of salt represents hyperosmotic shock, leading to a decrease in the tension of the plasma membrane. This has been shown to inhibit the activity of TORC2 (Riggi et al., 2018), an important activator of SPT, which facilitates the first and rate-limiting step of *de novo* sphingolipid biosynthesis. Consistent with this, sphingolipid catabolism enzymes are upregulated by salt stress in a manner dependent on the high-osmolarity glycogen (HOG) pathway, whereas sphingolipid biosynthesis enzymes are downregulated (Manzanares-Estreder et al., 2017). We therefore tested whether a targeted drop in sphingolipid levels was sufficient to induce the disintegration of eisosome remnants. To induce a general decrease in sphingolipid biosynthesis intermediates, we used the well-described SPT inhibitor myriocin (Miyake et al., 1995; Huang et al., 2012; Tanigawa et al., 2012; Pimentel et al., 2022). In the *pil1*Δ strain, the decreased SPT activity and resulting sphingolipid insufficiency induced dissolution of remnants and formation of Lsp1 eisosomes, an increase of mean

Journal of Cell Science (2023) 136, jcs260554. doi:10.1242/jcs.260554

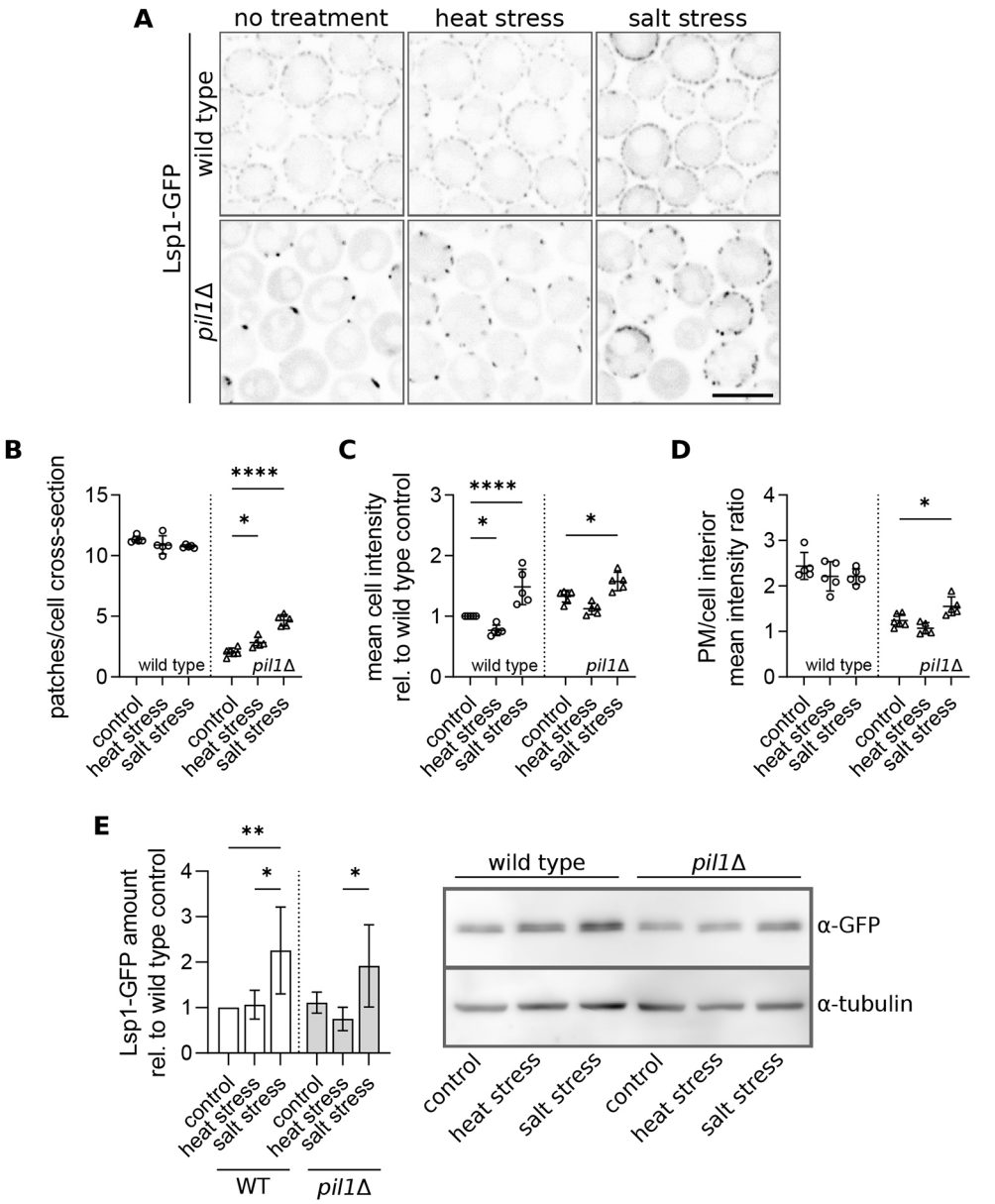

Fig. 1. Heat and salt stress induce the formation of Lsp1 foci in the plasma membrane. (A) Confocal fluorescence microscopy images (transversal sections) of *LSP1-GFP*-expressing yeast cells grown exponentially for 4 h at 28°C and subsequently shifted to 37°C for 2 h, or grown at 28°C in the presence of 1 M NaCl for 6 h to induce salt stress. Scale bar: 5 µm. (B–D) Quantification of the number of local Lsp1–GFP accumulations (patches) per cell cross-section (B), mean cell GFP intensity relative to the wild-type control (C) and the ratio of mean GFP fluorescence in the plasma membrane (PM) and the cell interior (D) in cells treated as in A. Data are presented as mean±s.d. from 4–5 biological replicates (circles, wild type; triangles, *pil1*Δ; 100–150 cells in each condition). (E) Western blot analysis of Lsp1–GFP protein amount in cells treated as in A, presented as mean±s.d. from 4–5 biological replicates. Representative membrane with tubulin as the loading control. **P*≤0.05, ***P*≤0.01, *****P*≤0.0001 (two-way ANOVA with Dunnett post test).

cellular Lsp1–GFP fluorescence and elevation of PM/intracellular GFP intensity ratio (Fig. 3C,D; Movie 1). This indicates an increase in Lsp1 protein abundance, consistent with previously reported overexpression of *LSP1* following cultivation in the presence of myriocin (Liu et al., 2013), and increased association of the Lsp1 protein with the plasma membrane. In addition, the mean intensity of the plasma membrane-associated Lsp1–GFP patches increased following myriocin treatment, while they became shorter (Fig. S2). Overall, the effect of myriocin treatment was comparable to that of salt stress, as expected. A decrease in the activity of the SPT can also be achieved genetically by exchanging the native *LCB1* gene, coding an essential subunit of the complex, for the temperature-sensitive *lcb1-100* allele carrying a missense mutation (Zanolari et al., 2000; Hearn et al., 2003). Analogous to what was seen with myriocin treatment of the *pil1ΔLCB1* strain, the non-stressed *pil1Δlcb1-100* cells formed Lsp1–GFP eisosomes, whereas their isogenic *pil1*Δ parent only had eisosome remnants (Fig. 3E; Fig. S2E).

As the addition of PHS and myriocin have opposite effects on the levels of cellular sphingolipids (Pimentel et al., 2022), it is quite curious that both induce the formation of Lsp1 eisosomes in *pil1*Δ cells. To get more insight into the regulation of this process, and to pinpoint specific sphingolipid pathway intermediates responsible for the changes in Lsp1–GFP localization we used aureobasidin A to inhibit Aur1, an enzyme converting ceramides into inositolphosphoceramides (Heidler and Radding, 1995; Nagiec et al., 1997). The effect of such inhibition is an accumulation of PHS and ceramide (analogous to exogenous PHS addition) and a decrease in the level of complex sphingolipids (as after myriocin treatment) (Nagiec et al., 1997; Schorling et al., 2001; Voynova et al., 2014). Surprisingly, this combined effect of aureobasidin A treatment had no discernible effect on Lsp1–GFP localization in either wild-type cells or the *pil1*Δ strain (Fig. 3; Fig. S2). This indicates that the formation of Lsp1 eisosomes in the response to stress is not connected to the level of a specific class of sphingolipids.

Therefore, we considered that the addition of either myriocin or PHS, and the use of the *lcb1-100* mutant allele all lead to downregulation of the activity of SPT, whereas aureobasidin A

Journal of Cell Science (2023) 136, jcs260554. doi:10.1242/jcs.260554

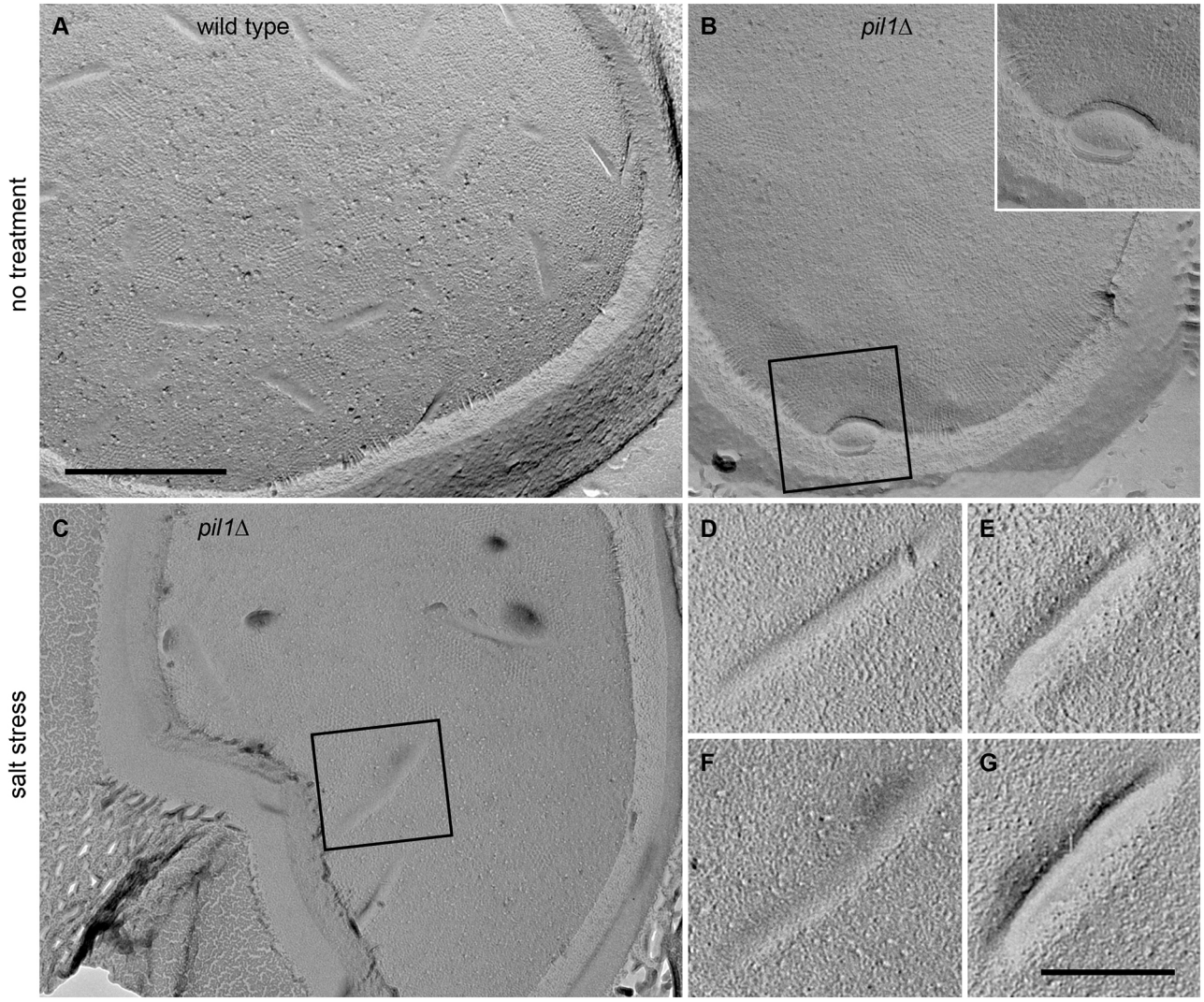

Fig. 2. Lsp1–GFP foci induced by salt stress are eisosomes. Freeze-fracture electron microscopy images of the plasma membrane (P-face) in the wild type (A; normal condition) and *pil1*Δ (B,C; normal condition and salt stress, respectively) yeast cells (unlabeled). Note the presence of membrane invaginations (furrows) in C. (D–G) Detailed view of furrows in *pil1*Δ cells exposed to salt stress (F corresponds to the area in the black square in C). Scale bars: 500 nm (A–C), 200 nm (D–G). Images representative of results from three experiments.

treatment does not. Myriocin and *lcb1-100* directly decrease the enzymatic activity of SPT (Miyake et al., 1995; Zanolari et al., 2000). Exogenous addition of PHS increases the pool of both LCBs (the products of SPT reaction) and complex sphingolipids (Pimentel et al., 2022), which regulate SPT activity via the MCC/eisosome→TORC2→SPT feedback loop (Fröhlich et al., 2009; Berchtold et al., 2012; Zahumenský et al., 2022). Our data, therefore, indicate a negative correlation between Lsp1 eisosome formation and the activity of SPT.

High osmolarity triggers formation of Lsp1 eisosomes

To uncover the underlying principle of Lsp1 eisosome formation in response to stress, we considered that heat stress (Dunayevich et al., 2018; Winkler et al., 2002), salt stress (Bermejo et al., 2008; Vallejo and Mayinger, 2015) and inhibition of sphingolipid synthesis (Tanigawa et al., 2012) all activate high-osmolarity glycerol (HOG) pathway. We therefore tested whether exposure of *pil1*Δ cells to high osmolarity induced by 1 M sorbitol, a known activator of the HOG pathway (García-Rodríguez et al., 2005), was sufficient to trigger the formation of Lsp1 eisosomes. Given that sorbitol induces transient phosphorylation of the cell wall integrity (CWI) pathway mitogen-activated protein kinase (MAPK) Slt2 45–60 min after addition (García-Rodríguez et al., 2005), we treated the cultures with sorbitol for 25 min to prevent possible HOG–CWI interference. The changes in Lsp1–GFP localization following sorbitol treatment were comparable to those produced by the cultivation of cells in the presence of 1 M NaCl (Fig. 4A–D; compare with Fig. 1). Specifically, eisosome remnants disintegrated and Lsp1 eisosomes were formed instead. These were distributed almost evenly along the plasma membrane. In the wild-type strain, the number of eisosomes was unaffected by sorbitol treatment (Fig. 4A,B). To completely exclude the possibility that the activation of the CWI pathway contributes to Lsp1 eisosome neogenesis, we treated the cultures with 100 µg/ml Calcofluor White, a known selective activator of the CWI pathway (García-Rodríguez et al., 2005). We found no effect on Lsp1–GFP localization in either *pil1*Δ cells or the wild-type cells, and conclude that cell wall stress does not induce eisosome remnant disassembly and Lsp1 eisosome formation (Fig. 4A–D).

Given that we discovered Lsp1 eisosome formation in *pil1*Δ cells in response to hyperosmotic stress, we tested whether the

Journal of Cell Science (2023) 136, jcs260554. doi:10.1242/jcs.260554

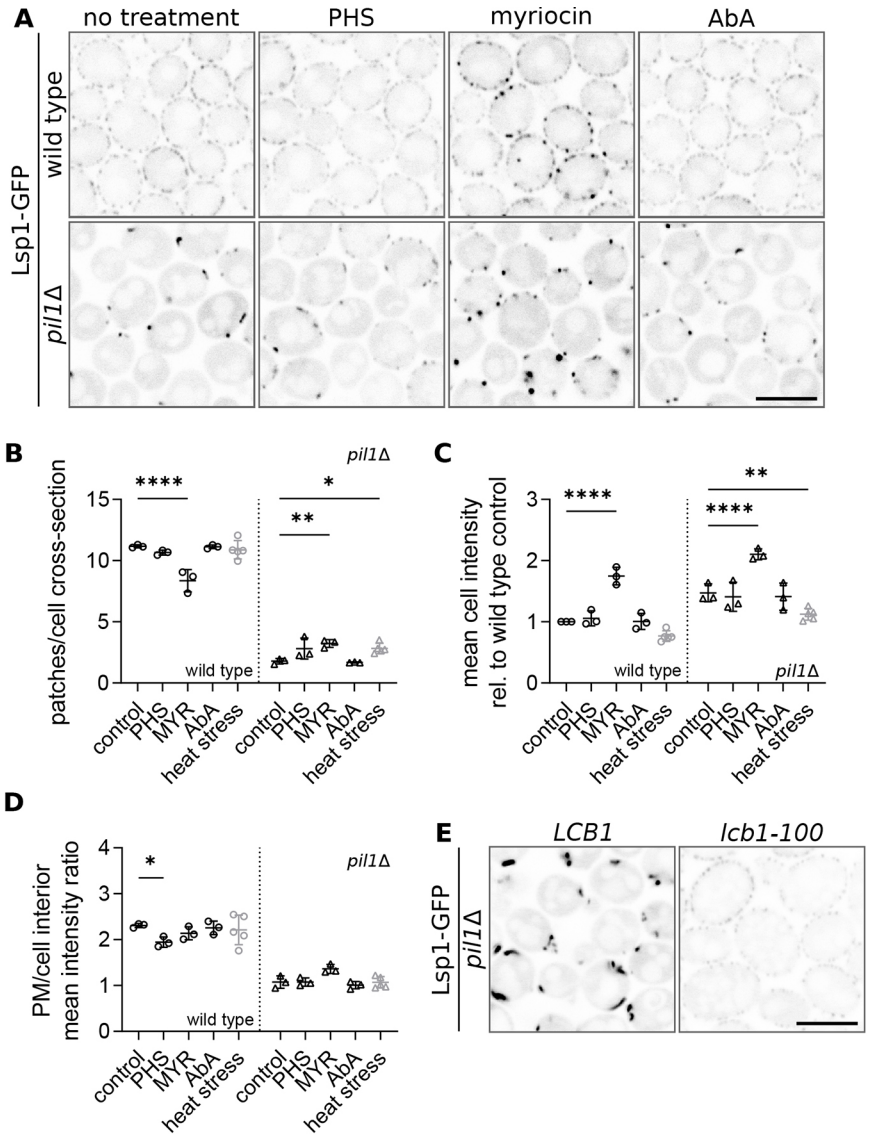

Fig. 3. Decrease in the activity of SPT induces the formation of Lsp1 eisosomes in the plasma membrane. (A) Confocal fluorescence microscopy images of *LSP1-GFP*-expressing yeast cells (BY4742 background) grown exponentially for 4 h at 28°C and treated with indicated chemicals for 2 h. (B–D) Quantification of the number of local Lsp1–GFP accumulations (patches) per cell cross-section (B), mean cell GFP intensity relative to the wild-type control (C) and the ratio of mean GFP fluorescence in the plasma membrane (PM) and the cell interior (D) in cells treated as in A. To facilitate direct comparison, data points for heat stress treatment (from Fig. 1) were included in the graphs. Data are presented as mean±s.d. from three biological replicates (circles, wild type; triangles, *pil1*Δ; 170–230 cells in each condition). *$P\leq0.05$, **$P\leq0.01$, ****$P\leq0.0001$ (two-way ANOVA with Dunnett post test). Data for PHS addition and heat stress from Fig. 1 were compared using an unpaired two-tailed *t*-test, which reported absence of significant difference. (E) Confocal fluorescence microscopy images of *LSP1-GFP*-expressing yeast cells (RH1800 background) grown exponentially for 5 h at 25°C. Transversal sections are presented in A and E. Scale bars: 5 µm. PHS, phytosphingosine, 10 µM; MYR, myriocin, 10 µM; AbA, aureobasidin A, 1 µg/ml.

HOG pathway is required for this process by the deletion of the MAPK gene *HOG1*. This had no significant effect on the Lsp1–GFP localization in either presence or absence of *PIL1*. Likewise, Lsp1–GFP localization changed in both strains following sorbitol addition in a manner comparable to strains expressing *HOG1*. Eisosome remnants disassembled and Lsp1 eisosomes were formed (Fig. S3). Our results indicate that the Hog1 MAPK is not required for the formation of Lsp1 eisosomes in response to hyperosmotic stress. If HOG pathway takes part in the process, then the step triggering eisosome formation lies upstream of Hog1.

The eisosome organization is regulated by the Pkh1 and Pkh2 kinase-mediated phosphorylation of Pil1 and Lsp1, which depends on the levels of long-chain sphingoid bases DHS and PHS (Walther et al., 2007; Luo et al., 2008; Baxter et al., 2011). Given that LCBs stimulate phosphorylation of the Lsp1 protein (Zhang et al., 2004), we expected to find decreased Lsp1 phosphorylation under conditions when SPT activity is lowered. Indeed, using a modified western blot protocol, which facilitates the separation of phosphorylated species, we found a decrease in Lsp1 phosphorylation in *pil1*Δ cells following hyperosmotic stress (Fig. 4E). We conclude that the remodeling of eisosome remnants into Lsp1 eisosomes in response to stress is regulated by phosphorylation of Lsp1.

Nce102 and Seg1 cooperate to mediate the association of Lsp1 with the plasma membrane

We found that Lsp1 in *S. cerevisiae* is able not only to participate in the assembly of the Pil1-organized eisosome but also to assemble the eisosome on its own, in the absence of Pil1, under certain conditions. We asked whether, in the absence of Pil1, Lsp1 was necessary for eisosome formation, and whether Lsp1 alone was sufficient to assemble eisosomes or requires other MCC/eisosome components.

To answer the first question, we followed the localization of Seg1–GFP, an enhancer of eisosome formation and stability (Seger et al., 2011; Moreira et al., 2012; Vaskovicova et al., 2015). In the wild-type strain, Seg1–GFP had a typical eisosome pattern at the plasma membrane (Fig. 5A). In the absence of *PIL1*, when remnants are formed instead of eisosomes, Seg1–GFP accumulated in eisosome remnants, as was the case for Lsp1 (compare with Figs 1, 3). Its mean cellular fluorescence intensity increased

Journal of Cell Science (2023) 136, jcs260554. doi:10.1242/jcs.260554

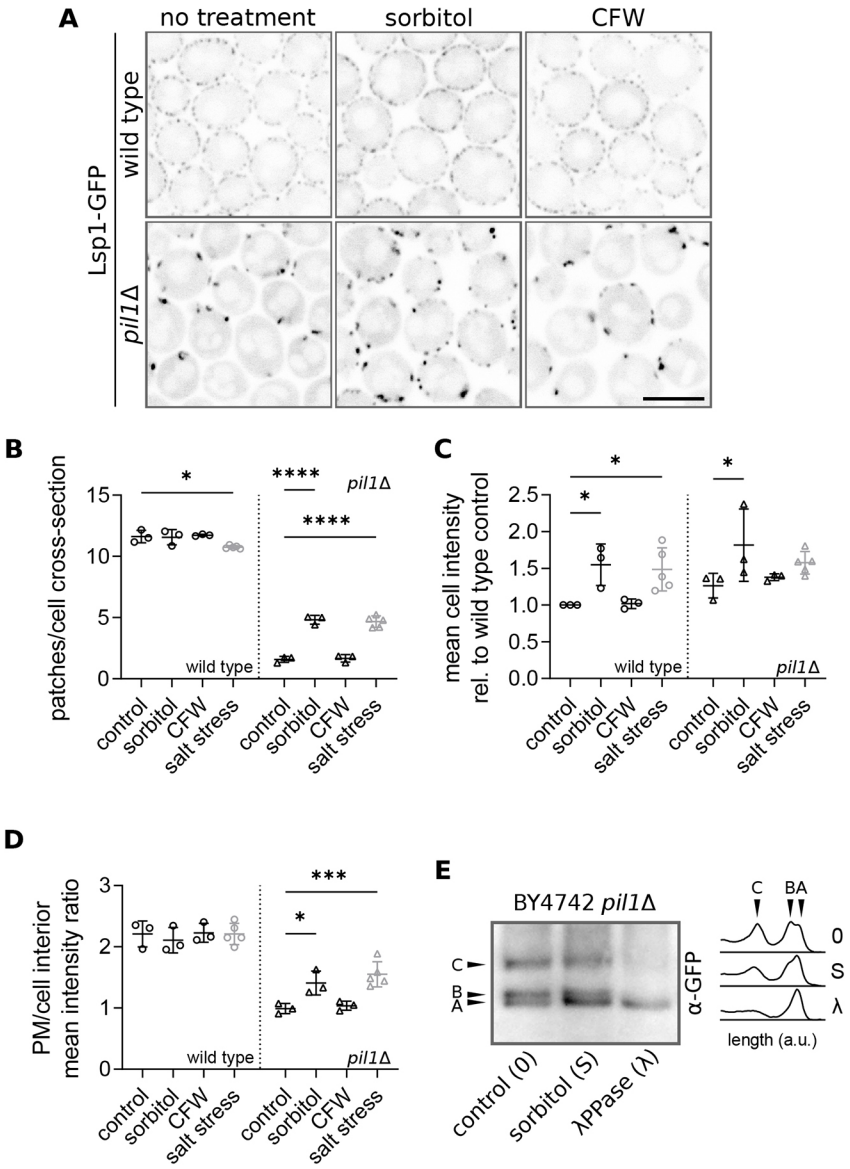

Fig. 4. Hyperosmotic stress induces Lsp1 eisosome formation. (A) Confocal fluorescence microscopy images (transversal sections) of *LSP1-GFP* expressing yeast cells grown exponentially for 6 h at 28°C and treated with indicated chemicals for 25 min. Scale bar: 5 µm. (B–D) Quantification of the number of local Lsp1–GFP accumulations (patches) per cell cross-section (B), mean cell GFP intensity relative to the wild-type control (C) and the ratio of mean GFP fluorescence in the plasma membrane (PM) and the cell interior (D) in cells treated as in A. To facilitate direct comparison, data points for salt stress treatment (from Fig. 1) were included in the graphs. Data are presented as mean±s.d. from three biological replicates (circles, wild type; triangles, *pil1*Δ; 85–130 cells in each condition). **P*≤0.05, *****P*≤0.0001 (two-way ANOVA with Dunnett post test). Data for osmotic stress and salt stress from Fig. 1 were compared using an unpaired two-tailed *t*-test, which reported absence of significant difference. (E) Western blot analysis of Lsp1–GFP phosphorylation change in response to a decrease in SPT activity. We detected Lsp1–GFP in cell protein extracts prepared from BY4742-derived *LSP1-GFP*-expressing *pil1*Δ cells grown exponentially for 6 h and treated either with nothing (lane 1; 0) or with 1 M sorbitol (lane 2; S) for 25 min. To verify that the multiple detection bands originate in phosphorylation, the sample was treated with λ-phosphatase (λPPase or λ; lane 3). A representative membrane from seven repeats is shown together with intensity profiles measured along lines perpendicular to the protein bands in a top-to-bottom direction (Fiji). The thickness of the lines corresponded to the width of the bands. A, B, C denote one non-phosphorylated and two phosphorylated bands, respectively; annotation based on previous reports (Luo et al., 2008). Sorbitol, 1 M; CFW, Calcofluor White, 100 µg/ml.

compared to that in the wild type (Fig. 5A,C). The deletion of *LSP1*, on the other hand, caused no discernible effect on the localization of Seg1–GFP. In the absence of both core eisosome components, Seg1–GFP localized almost exclusively into the cytoplasm with a very limited number of faint plasma membrane-associated patches and eisosome remnants (Fig. 5A,B,D). When cells were cultivated in the presence of 1 M NaCl, there was no change in the Seg1–GFP distribution when Pil1 was present. In the absence of Pil1, *LSP1* expression was required to enhance the association of Seg1 with the plasma membrane. In the *pil1*Δ cells, Seg1–GFP reformed from eisosome remnants into multiple well-defined plasma membrane foci (Fig. 5A,B), where it invariably colocalized with Lsp1 (Fig. 5E). In contrast, in the *pil1*Δ*lsp1*Δ strain, a change in Seg1 distribution induced by the salt stress was not clearly discernible, mainly because the plasma membrane-associated fraction of the protein remained low. Eisosome remnants could be seen even in stressed cells (Fig. 5A,B). We, therefore, conclude that in the absence of Pil1, Lsp1 is necessary for eisosome assembly during the stress response. The presence of Seg1 foci in the *pil1*Δ*lsp1*Δ strain is consistent with the idea that recruitment of Seg1 to the plasma membrane during eisosome assembly precedes that of Pil1 and Lsp1 and provides a platform for the assembly of other eisosome components (Moreira et al., 2012).

To answer the question of which proteins are required for eisosome formation in the absence of Pil1, we focused on two proteins known to promote eisosome stability across fungal species, the eisosome constituent Seg1 (Seger et al., 2011; Moreira et al., 2012; Kabeche et al., 2014; Vaskovicova et al., 2015) and the MCC protein Nce102, the absence of which has been shown to significantly reduce the eisosome number (Fröhlich et al., 2009; Loibl et al., 2010; Kabeche et al., 2011; Athanasopoulos et al., 2015). As expected, the deletion of either *SEG1* or *NCE102* resulted in a decrease, but not complete absence, of Lsp1–GFP foci in both wild-type and the *pil1*Δ background in the absence of stress (Fig. 6A,B). The mean cellular Lsp1–GFP fluorescence intensity was unaffected by these deletions (Fig. 6C). In the *pil1*Δ background, salt stress induced the formation of Lsp1 eisosomes in both *seg1*Δ and *nce102*Δ mutants, but to a lesser degree than in the strain only lacking *PIL1*, whereas it did not affect the mean Lsp1–GFP intensity in these strains. In contrast, the mean cellular

Journal of Cell Science (2023) 136, jcs260554. doi:10.1242/jcs.260554

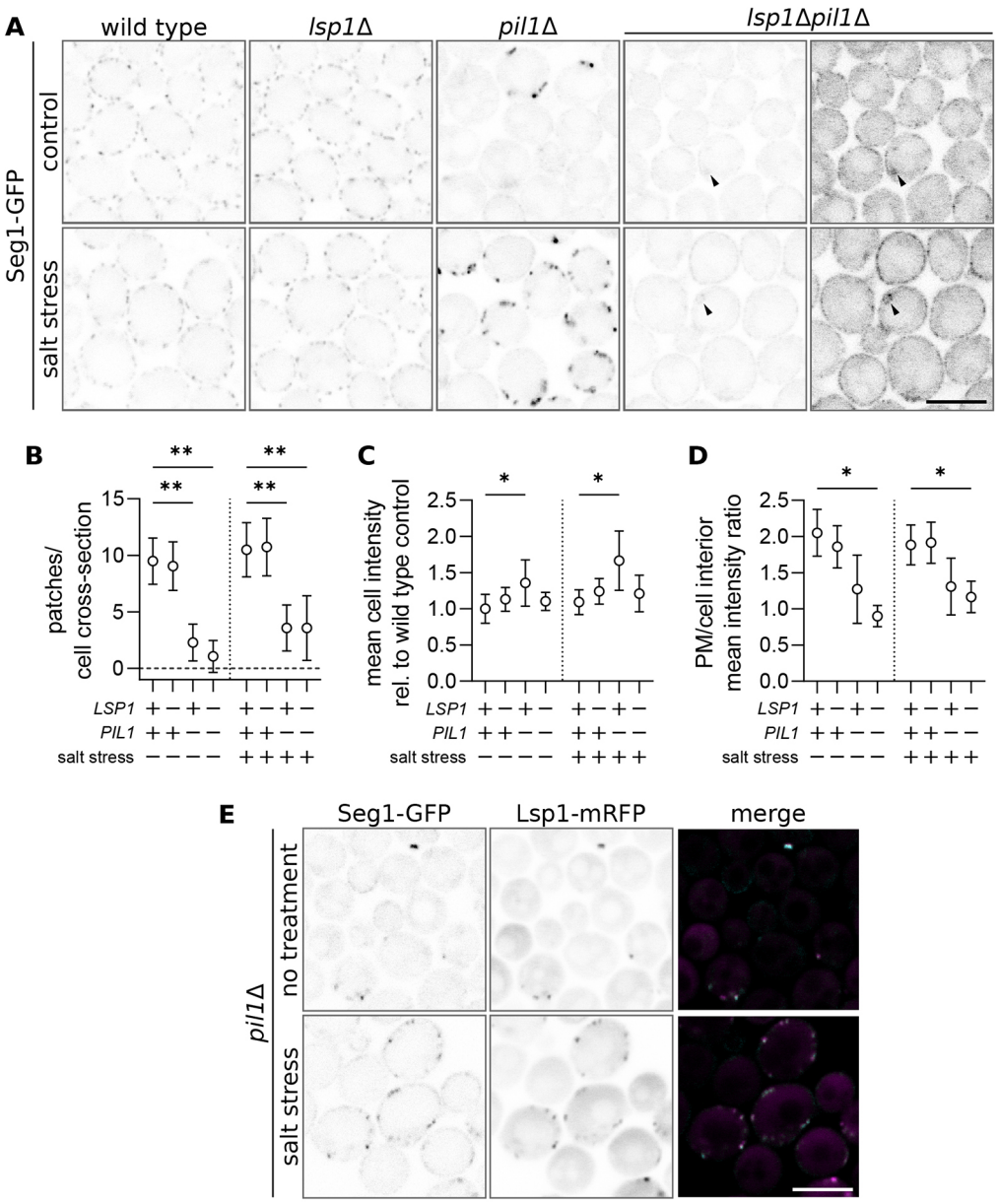

Fig. 5. In the absence of Pil1, Lsp1 is required for eisosome formation in response to stress. (A) Confocal fluorescence microscopy images (transversal sections) of yeast cells expressing *SEG1-GFP* grown exponentially for 6 h at 28°C either in the presence or absence of 1 M NaCl to induce salt stress. For the *lsp1Δpil1Δ* strain, images are shown also with separately adjusted contrast for better visibility of plasma membrane localization of Seg1–GFP. Arrowheads indicate eisosome remnants in the *lsp1Δpil1Δ* strain. Scale bar: 5 µm. (B–D) Quantification of the number of local Seg1–GFP accumulations (patches) per cell cross-section (B), mean cell GFP intensity relative to the wild-type control (C) and the ratio of mean GFP fluorescence in the plasma membrane (PM) and the cell interior (D) in cells treated as in A. Data are presented as mean±s.d. from a single experiment (170–230 cells in each condition). *$P\leq0.05$, **$P\leq0.01$ (two-way ANOVA with Dunnett post test). (E) Confocal fluorescence microscopy images (transversal sections) of yeast cells expressing *SEG1-GFP* and *LSP1-mRFP* grown exponentially for 6 h at 28°C either in the presence or absence of 1 M NaCl to induce salt stress. Scale bar: 5 µm. A representative image of three independent experiments is shown.

Lsp1–GFP intensity increased as a result of the simultaneous deletion of *SEG1* and *NCE102* in the *pil1*Δ background. However, the formation of Lsp1–GFP foci at the plasma membrane was almost completely abolished and was not induced by salt stress in this strain (Fig. 6). Our results, therefore, indicate that in the absence of Pil1, Lsp1 alone is not sufficient to form eisosomes in response to stress, but requires other proteins, either Seg1 or Nce102.

Stress resistance in the absence of the eisosome

The physiological role of the eisosome has not yet been fully elucidated. The existence of paralogous genes in the *S. cerevisiae* genome, which have arisen from whole genome duplication during evolution, has contributed significantly to this failure. In many cases, these homologs either partially or completely substitute for each other, resulting in the masking of phenotypes. Above, we constructed a strain lacking the *PIL1*, *SEG1* and *NCE102* genes, which appears to be the minimum requirement for a strain devoid of both eisosomes and eisosome remnants that do not form even when cells are exposed to stress.

To investigate the physiological function of the eisosome under stress, we tested the growth of mutant strains described above under various stress conditions. When grown at the suboptimal 37°C temperature, the viability of the studied strains was not severely affected. Slightly reduced growth was detected in *seg1*Δ, *seg1Δpil1*Δ and *seg1Δnce102*Δ strains (Fig. 7A). When cells were grown in the presence of 1 M NaCl, the absence of either Pil1 or Seg1 decreased the viability of the cells, but the effect was again small. Cultivation of cultures exposed to salt stress at 37°C significantly exacerbated the observed defects. Under conditions of heat stress, the sensitivity of the tested mutant strains to high salt exposure can be summarized as follows: in the absence of Pil1, Nce102 presence causes salt stress sensitivity. In the presence of Pil1, Seg1 confers salt stress resistance. This phenotype is not solely due to misregulation of the sphingolipid synthesis, as the absence of Pil1 induced resistance to 0.5 µg/ml of myriocin independently of *NCE102* and *SEG1* genes. Increasing the cultivation temperature to 37°C and increasing the myriocin concentration had an additive effect, as expected. This is exemplified well by the similarity of

Journal of Cell Science (2023) 136, jcs260554. doi:10.1242/jcs.260554

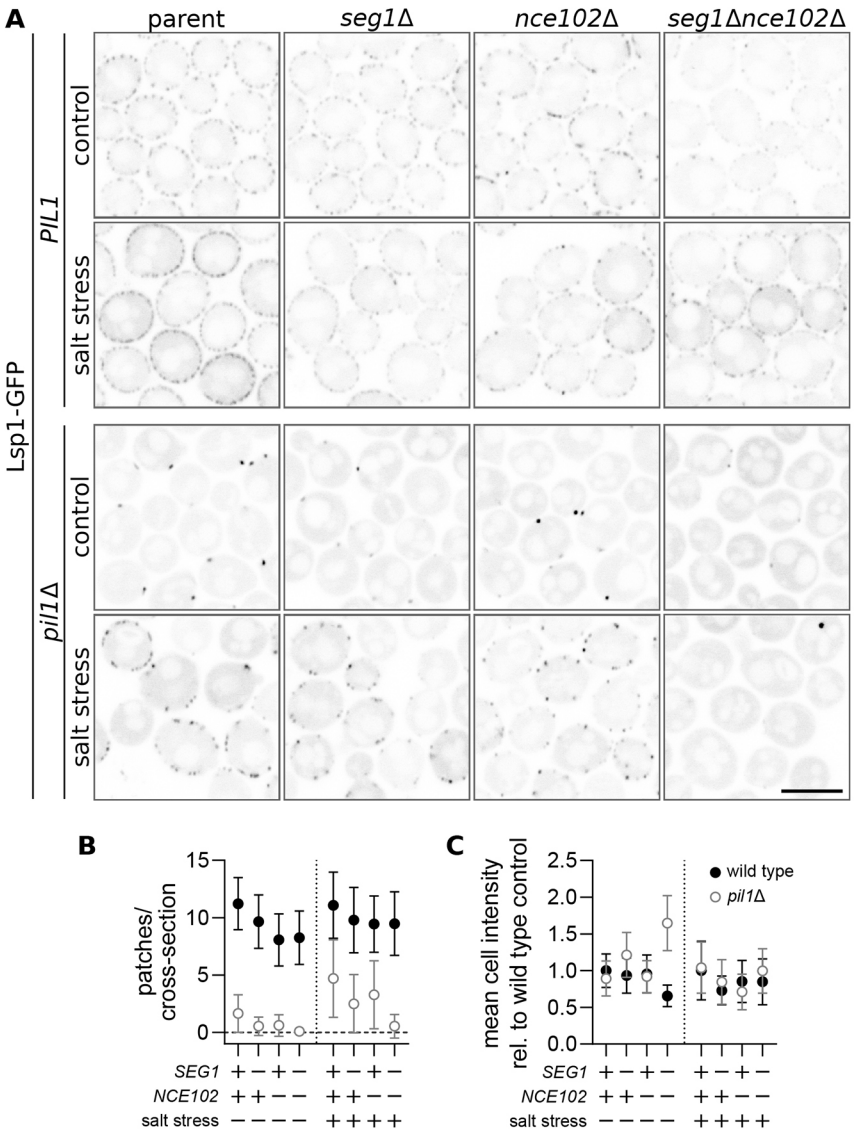

Fig. 6. Nce102 and Seg1 cooperate to mediate the association of Lsp1 with the plasma membrane. (A) Confocal fluorescence microscopy images (transversal sections) of yeast cells expressing *LSP1-GFP* (A) grown exponentially for 6 h at 28°C either in the presence or absence of 1 M NaCl. Scale bar: 5 µm. (B,C) Quantification of the number of local Lsp1–GFP accumulations (patches) per cell cross-section (B), and mean cell intensity relative to the wild-type control (C) in cells treated as in A. Data are presented as mean±s.d. from a single experiment (black circles, wild type; white circles, *pil1*Δ; 170–230 cells in each condition).

growth of the mutants exposed to 0.5 µg/ml myriocin at 28°C, on one hand, and to 0.25 µg/ml myriocin at 37°C, on the other hand (Fig. 7A). We conclude that Pil1, Seg1 and Nce102 cooperate to coordinate the yeast halotolerance. When all three are absent, the cells are, like wild-type, insensitive to high salt even under conditions of heat stress. To get more insight into the physiological role of the eisosome, we performed a corresponding series of experiments also with the *lsp1*Δ*pil1*Δ strain, which does not form eisosomes. Unlike the *seg1*Δ*nce102*Δ*pil1*Δ strain, however, it has eisosome remnants (Fig. 5A). Under all tested conditions, deletion of *LSP1* in any background did not change the phenotype of its isogenic parent strain.

Complete absence of eisosomes induces changes in lipid metabolism, oxidative phosphorylation, the cell cycle and MAPK signaling

Our data indicate that the newly constructed eisosome-less *seg1*Δ*nce102*Δ*pil1*Δ strain has growth phenotypes that are distinct from both those of the wild type and the *pil1*Δ strain. To obtain a better understanding of the underlying causes of these differences, we compared the whole transcriptome of the three strains using next-generation sequencing (NGS). To get an initial insight into the data, we performed principal component analysis (PCA), which analyzes correlations among the samples and creates a plot in which samples with similar expression profiles cluster together. Although the biological replicates of the wild-type and *pil1*Δ strain overlapped, there was a cluster where the *seg1*Δ*nce102*Δ*pil1*Δ strain clearly separated from the other samples (Fig. 8A). This indicates that although the expression profiles of wild-type and the *pil1*Δ strain are comparable, there is a significant difference in the transcriptome of the *seg1*Δ*nce102*Δ*pil1*Δ strain.

Consistently, although in-depth analysis reported no differentially expressed genes (DEGs) ($|\log_2\text{FoldChange}|>1$; adjusted $P<0.05$) in the *pil1*Δ strain, there were 1069 DEGs in the triple deletion mutant when compared to the wild type. A total of 635 of these genes were downregulated, whereas 434 genes, including *LSP1* (consistent with the mean cellular GFP intensity increase shown in Fig. 6A,C), were upregulated (Fig. 8B,C; Table S3). Performing Gene Set Enrichment Analysis (GSEA) on KEGG (Kyoto Encyclopedia of Genes and Genomes) pathways revealed significant changes (adjusted $P<0.05$) in 15 pathways/processes (Fig. 8D,E). The most affected were oxidative phosphorylation and tricarboxylic acid cycle (upregulated), and DNA replication, ribosome biogenesis and cell cycle (downregulated).

Journal of Cell Science (2023) 136, jcs260554. doi:10.1242/jcs.260554

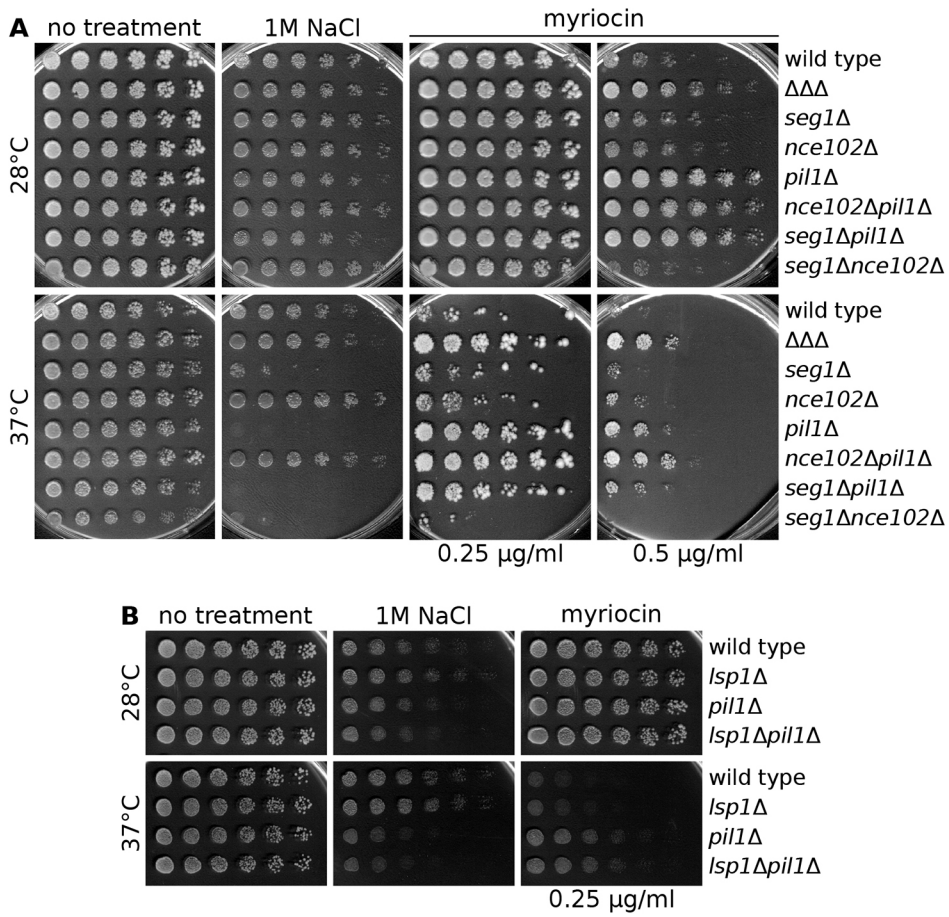

Fig. 7. Pil1, Seg1 and Nce102 cooperate to coordinate the yeast halotolerance. (A,B) Indicated unlabeled yeast mutant strains were cultivated as described in the Materials and Methods and replica-plated on YPD plates containing indicated chemicals. These were then incubated at indicated temperatures. The control for the myriocin-containing plates is shown in A. ΔΔΔ, *seg1Δnce102Δpil1Δ*. Images representative of results from four experiments.

DISCUSSION

The core eisosome proteins Pil1 and Lsp1 share ∼72% sequence identity. However, their contribution to the assembly of the hemitubular scaffold of the eisosome is remarkably different. Under normal laboratory conditions, eisosomes collapse into eisosome remnants when Pil1 is not present in the cell. The absence of Lsp1, on the other hand, has no apparent effect on eisosome morphogenesis (Walther et al., 2006; Grossmann et al., 2007; Olivera-Couto et al., 2011; Deng et al., 2009). It was therefore believed that, on its own, Lsp1 was insufficient to organize the eisosomes. In our present study, we report that under certain conditions, such as hyperosmotic stress, the eisosome remnants of *pil1*Δ cells disintegrate and eisosomes are formed even without Pil1. These Lsp1 eisosomes require the integral MCC protein Nce102 and the eisosome component Seg1 for their formation.

It has been previously reported that hyperosmotic stress, which induces cell shrinkage, induces morphological changes in the MCC/eisosome microdomain. The resulting decrease in membrane tension promotes deepening of eisosomes (Schaber et al., 2010; Dupont et al., 2010; Appadurai et al., 2020) and the accumulation of phosphatidylinositol 4,5-bisphosphate (PIP_2) in the furrows (Riggi et al., 2018). In the absence of Pil1, the distribution of PIP_2 in the plasma membrane changes from being quite punctate to being more homogeneous, and the lipid becomes more accessible to the binding of the GFP–2xPH_{PLC} probe (Fröhlich et al., 2014). Hyperosmotic stress induces the formation of PIP_2 clusters in the plasma membrane (Kabeche et al., 2015; Riggi et al., 2018). It is plausible that these clusters provide a binding platform for Seg1 [via its BAR and PH domains (Moreira et al., 2012)] and Lsp1 (via the BAR domain; Ziółkowska et al., 2011), and that the interaction of these proteins further enhances their binding to the plasma membrane. This points to the general mechanism of eisosome biogenesis. Correspondingly, we show that heat stress is another inducer of Lsp1 eisosome formation in the absence of Pil1. Heat stress has been shown to stimulate a transient increase of cellular PIP_2 (Desrivières et al., 1998). The transiency of this change might explain why heat stress is a weaker inducer of Lsp1 eisosome formation than salt or hyperosmotic stress. Further support for the PIP_2-based mechanism of eisosome formation comes from our observation that under salt stress conditions, the plasma membrane association of Seg1 slightly increases even in the strain lacking both eisosome organizers, Pil1 and Lsp1 (Fig. 5).

Pil1, Nce102 and other proteins are known to leave the MCC/eisosome when the cellular need for sphingolipids is not met (Fröhlich et al., 2009; Zahumenský et al., 2022), leading to destabilization of the whole microdomain. By contrast, Lsp1 is required for elongation of eisosomes and an increase in their number in the stationary phase (Gournas et al., 2018), that is, in a respiring culture with limited nutrient supply. It should be emphasized here that our observation of increased eisosome assembly in myriocin-treated *pil1*Δ cells (Fig. 3) is not contradictory to the earlier report of partial eisosome disassembly following myriocin treatment in the wild-type cells (Fröhlich et al., 2009). The authors of the cited study identified the release of Nce102 as the primary reason for the decrease in the eisosome number. We showed recently that this occurs specifically during cytokinesis, which the cells undergo in the presence of myriocin (Zahumenský et al., 2022). A decreased amount of Nce102 in the MCC/eisosome, reporting here the local

Journal of Cell Science (2023) 136, jcs260554. doi:10.1242/jcs.260554

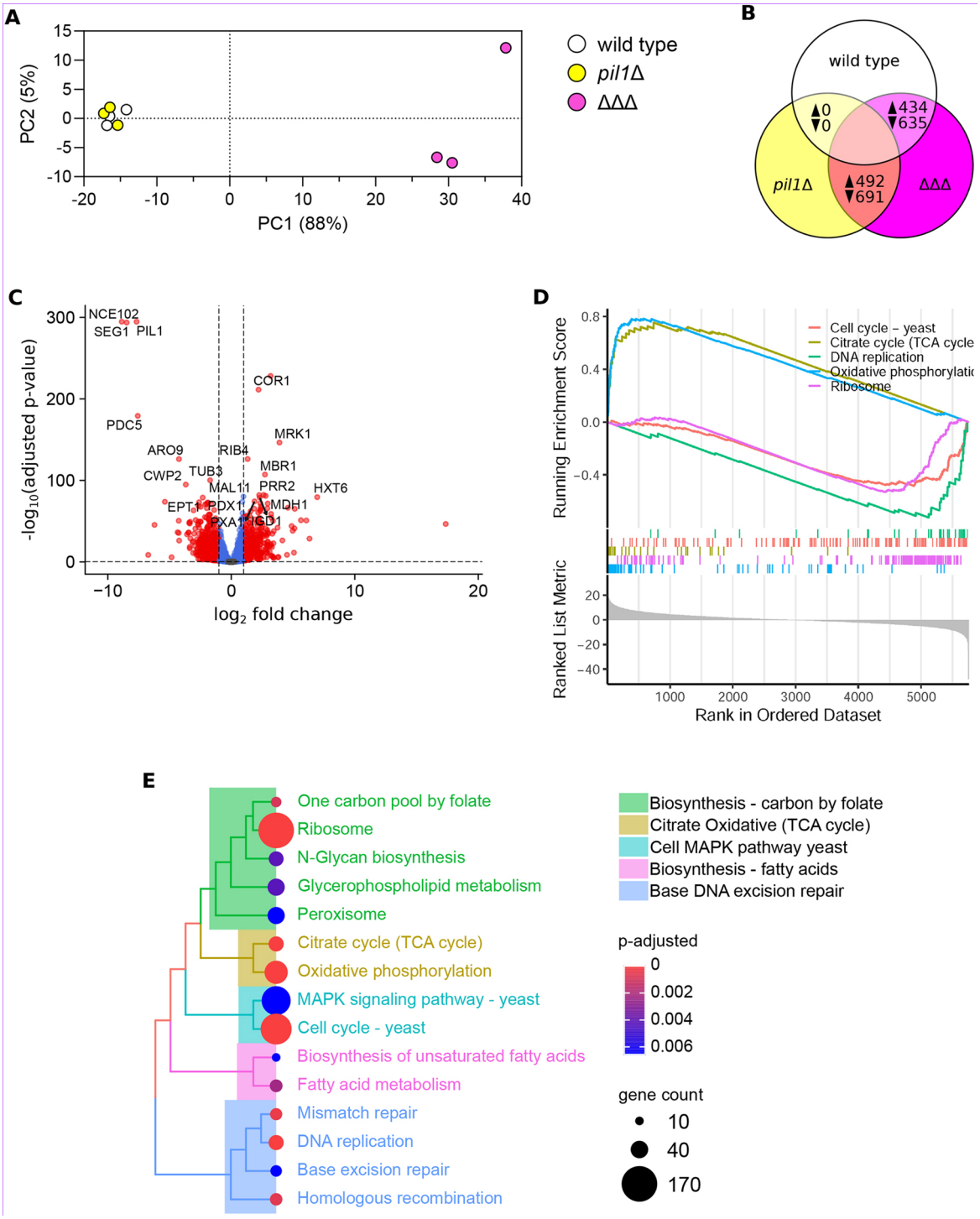

Fig. 8. Absence of the eisosome causes general transcriptome remodeling of the cell. Indicated yeast strains were cultivated in SC for 24 h, followed by isolation of total RNA and mRNA enrichment using polyA selection for library preparation. Three biological replicates were performed for each strain. (A) Principal component analysis (PCA). (B) Venn diagrams displaying number of DEGs between indicated strains (*pil1*Δ versus wild type, *seg1*Δ*nce102*Δ*pil1*Δ versus wild type, and *seg1*Δ*nce102*Δ*pil1*Δ versus *pil1*Δ); up- and down-pointing triangles represent up- and down-regulated genes, respectively. (C) Volcano plot of differentially expressed genes in *seg1*Δ*nce102*Δ*pil1*Δ compared to wild type. (D) Gene Set Enrichment Analysis (GSEA) of the NGS data shown in C. The five most affected KEGG pathways and processes are displayed. (E) Hierarchical clustering of KEGG pathways and processes displayed in C. ΔΔΔ, *seg1*Δ*nce102*Δ*pil1*Δ; thresholds for differential expression: $|\log_2\text{FoldChange}|>1$; adjusted $P<0.05$. normalized gene expression counts were used in B and C; the normalization method was median of ratios (inherent in DESeq2); rlog2-transformed gene expression counts were used in A, D and E.

lack of sphingolipids, mimics the situation in the *nce102*Δ mutant, which exhibits a decreased eisosome number (Fröhlich et al., 2009). The number of Lsp1 eisosomes formed in the absence of Pil1 under the stress conditions or in myriocin-treated cells (Figs 1 and 3) is significantly lower compared to that in the wild-type cells. It could be that Lsp1-stabilized eisosomes are those which persisted after the

Journal of Cell Science (2023) 136, jcs260554. doi:10.1242/jcs.260554

myriocin treatment in both cases, either in the wild-type or *pil1*Δ strain. If so, the only difference would be that, in the absence of Pil1, Lsp1 eisosomes are newly formed in the plasma membrane, while in the presence of Pil1, dissociation of Pil1 and increased association of Lsp1 with the plasma membrane following the myriocin treatment would occur together.

We report that the formation of Lsp1 eisosomes in response to stress requires the presence of the integral MCC protein Nce102 and the soluble eisosome component Seg1. The Lsp1 eisosomes are less abundant in the absence of either and all but completely absent when neither is present. Our microscopy (Fig. 6C) and NGS (Table S1) data indicate an increase in the level of Lsp1 in the *seg1*Δ*nce102*Δ*pil1*Δ strain, which suggests that the cell increases the production of available eisosome components in the attempt to build the structure. Consistent with this, our NGS data indicate downregulation of the *MAK3* gene, deletion of which in otherwise wild-type cells leads to over-assembly of eisosomes and their aberrant elongation (Grossmann et al., 2008; Malinsky et al., 2010). Our NGS analysis reported that there are no significant differences in the transcriptome of the *pil1*Δ strain compared to wild type. This corresponds very well with the fact that this strain exhibits only weak phenotypes when cultures are grown under normal laboratory conditions.

Analyzing the *seg1*Δ*nce102*Δ*pil1*Δ strain, the plasma membrane of which is devoid of eisosomes under both normal and stress conditions, we found that its stress resistance differs from both the wild-type cells and the *pil1*Δ strain. Like the *pil1*Δ, the triple mutant shows increased resistance to myriocin compared to the wild type. Unlike the *pil1*Δ, however, the halotolerance of the triple mutant does not differ from the wild type. In a recent study, a different eisosome-lacking strain has been described (Sakata et al., 2022). In this strain, genes coding both Nce102-like proteins (Nce102 and Fhn1) and four MCC-localizing members of the Sur7 family (Sur7, Pun1, Fmp45 and Ynl194c) were removed in addition to *PIL1*. The resulting strain had elevated sensitivity to salt stress and the membrane-disruptive chemical SDS, which the authors ascribed to hyperactive TORC2 signaling. Our simpler eisosome-lacking mutant, and also the *nce102*Δ*pil1*Δ strain, showed no sensitivity to either salt stress (Fig. 7A) nor SDS (data not shown). Keeping in mind low *FHN1* expression levels under given conditions (Loibl et al., 2010), this difference indicates a possible protective role of Sur7 family proteins in salt stress.

We found that the Hog1 MAPK is not required for the formation of Lsp1 eisosomes in *pil1*Δ cells in response to hyperosmotic stress. This contrasts with the known existence of a functional connection between the eisosome-regulated CWI pathway and the eisosome component Pil1. Specifically, the CWI MAPK Slt2 has been shown to phosphorylate Pil1, and thus provide a feedback loop between the pathway activation and eisosome assembly (Mascaraque et al., 2013). On the other hand, the absence of the MAPK of the HOG pathway does not impair the eisosome assembly, indicating that another (upstream) step of the pathway possesses an eisosome-related regulatory function. Further investigation will be necessary to identify this regulator. At the moment, we can only speculate about the role of the Sho1 branch of the HOG pathway, which includes lateral rearrangement (clustering) of the receptor components in the plasma membrane upon activation (Tatebayashi et al., 2007, 2015).

Previously, the MCC/eisosome has been linked to the regulation of nutrient transporter turnover (Grossmann et al., 2007; Gournas et al., 2017; Busto et al., 2018), RNA degradation (Grousl et al., 2015; Vaškovičová et al., 2017) and sphingolipid biosynthesis (Fröhlich et al., 2009; Berchtold et al., 2012; Zahumenský et al., 2022). The construction of a strain that forms neither eisosomes nor eisosome remnants allowed us to identify novel functional connections between the MCC/eisosome microdomain and essential cellular processes. Transcriptome analysis of this strain revealed significant changes in the metabolism of lipids, oxidative phosphorylation, MAPK signaling and cell cycle progression, clearly indicating novel avenues to be explored in future eisosome research.

MATERIALS AND METHODS

Strains and growth conditions

S. cerevisiae strains used in this study are listed in Table S1. Yeast cells were incubated in a complete synthetic (SC; 0.17% yeast nitrogen base without amino acids and ammonium sulfate, 0.5% ammonium sulfate, 2% glucose, amino acids) or rich medium (YPD; 2% peptone, 1% yeast extract, 2% glucose) at 28°C on a shaker. In all experiments including the *lcb1-100* allele-containing strain, the cultivation was performed at 25°C. For assessment of the effects of chemical stress on Lsp1–GFP localization, cultures were grown in SC medium as described above for 4 h, followed by the addition of aureobasidin A (1 mg/ml ethanol stock), myriocin (2 mg/ml methanol stock; Sigma, M1177), or phytosphingosine (PHS, 5 mg/ml ethanol stock; Sigma, P2795) to desired concentrations and additional 2-h cultivation. In the case of salt stress, cells were cultivated in the presence of 1 M NaCl for 6 h. Hyperosmotic stress and cell wall stress were induced by cultivating the cells for 6 h in SC, followed by their 25-min exposure to 1 M sorbitol (added as 0.91 g powder to 5 ml of culture) or 100 µg/ml Calcofluor White (1 mg/ml stock), respectively. All chemicals were purchased from Merck. For heat stress, cells were grown for 4 h as described above, then shifted from 28°C to 37°C. For electron microscopy preparations, the cells were cultured in YPD. For propagation of plasmids, *Escherichia coli* strain XL1-Blue (Stratagene, San Diego, CA, USA) was used. Bacterial strains were incubated in LB medium (1% tryptone, 0.5% yeast extract, 1% NaCl) supplemented with ampicillin (100 µg/ml) for selection of transformants.

Plasmids

Construction of the YIp128-*SEG1-GFP* plasmid has been described previously (Vaskovicova et al., 2015). The YIp128-*LSP1-GFP* plasmid was constructed as follows. The gene of interest was inserted as a HindIII-BamHI fragment into the YIp128-GFP plasmid. Before the transformation, the plasmid was linearized by digestion with the PmlI restriction enzyme. The pKT128-*LSP1-GFP* cassette was amplified by PCR from the pKT128 plasmid (*EUROSCARF*, P30174) using the primers *LSP1*-gnmtag_F, 5′-ATGTTAGTCAAAACGGTCATACCTCCGGTTCTGAAAACATCCG-GATCGGTGACGGTGCTGG-3′ and *LSP1*-gnmtag_R, 5′-TAGGTAGA-CACGAGCTGGTGAAAAACAAGCACAATATAGAAAGGTTCGCAT-CGATGAATTCGAGCTCG-3′. The obtained fragment was used to transform the yeast BY4742 strain (*EUROSCARF*). Candidate colonies were selected on histidine drop-out plates. The pCM225-*LSP1-GFP* cassette was amplified by PCR from the pCM225 plasmid (*EUROSCARF*, P30342) using the primers *LSP1*_pCM225_ctrl_F, AAGATGCAACG-GCTAAATCGCAATATATAAACAGGTGAGATAGCAGCTGAAGCT-TCGTACGC-3′ and *LSP1*_pCM225_ctrl_R, 5′-AGCCGTTGGAGCTC-TTTGATTTCTTAAAGAGTAAGTTCTGTGCATATAGGCCACTAGT-GGATCTG-3′. The obtained fragment was used to transform the yeast BY4742 strain (*EUROSCARF*). Candidate colonies were selected on YPD supplemented with kanamycin G418 (100 µg/ml; Gibco, 11815-024) for the selection of transformants. The pFA6a-*natMX6_PIL1* deletion cassette was amplified by PCR from the pFA6a-*natMX6* plasmid (*EUROSCARF*, P30437) using the primers *PIL1*_del_pFA6a_F, 5′-TATTGCAAAGTGA-AGAATATATCAGCATCAAGTATATAGTCGGATCCCCGGGTTAAT-TAA-3′ and *PIL1*_del_pFA6a_R, 5′-TTAATTAAAAGAGATTAATTA-GTATGGTAACTTGTTCTTTTCTGCTGGGAATTCGAGCTCGTTTAA-AC-3′. The obtained fragment was transformed into strains Y1214, Y1233, Y1234 and Y1417 (Table S1). Subsequently, the transformants were selected on YPD supplemented with nourseothricin (100 µg/ml; Jena

Bioscience AB102L). The presence of the pFA6a-*natMX6_PIL1* deletion cassette was verified by colony PCR.

Mating, diploid selection and sporulation

The double- and triple-deletion strains were obtained by mating suitable single- and double-deletion strains (Table S2) and subsequent sporulation and tetrad dissection. Mutants were selected with the help of the fluorescence microscopy as non-fluorescing colonies. Successful deletions were then verified by PCR.

Confocal microscopy

Living yeast cells grown in SC medium were concentrated by a brief centrifugation (1430 ***g*** for 2 min), immobilized on a 0.17 mM cover glass by a thin film of 1% agarose prepared in 50 mM potassium phosphate buffer (pH 6.3) and imaged using LSM 880 (Zeiss; 100× PlanApochromat oil-immersion objective; NA=1.4) laser scanning confocal microscope. The fluorescence signal of GFP (excitation 488 nm; Ar laser) and mRFP/mCherry (excitation 561 nm; solid-state laser) was detected using the 493–550 nm and 578–696 nm band-pass emission filters (Zeiss), respectively.

Preparation of freeze-fracture replicas and electron microscopy

Cells from an overnight culture were harvested by brief centrifugation (1 min at 1500 ***g***) and washed in 50 mM potassium phosphate buffer (pH 5.5). A 2 µl aliquot of the concentrated cell suspension was loaded onto a gold carrier and frozen rapidly in liquid nitrogen. The sample was cut with a cold knife ($T \leq -185$°C), etched for 4 min (−97°C; pressure≤1.3105 Pa) in a CFE-50 freeze-etch unit (Cressington, Watford, UK), shadowed (1 nm Pt/C, 45°C; 10 nm C, 90°C), and cleaned in fresh 70% H_2SO_4 for 16 h. Air-dried sample surface replicas were examined using an FEI Morgagni 268(D) transmission electron microscope at 80 kV. Images were captured with a MegaView II CCD camera (Olympus Corp., Münster, Germany).

Western blot analysis

Yeast cells were grown for 6 h and harvested by centrifugation (1430 ***g*** for 2 min). The pellet was resuspended in distilled water, precipitated by the addition of 0.6 ml of 100% (w/v) tricarboxylic acid (TCA) and kept on ice for 15 min before being centrifuged (5 min, 2460 ***g***, 4°C). The supernatant was aspirated and the remaining pellet was washed twice with cold acetone. After spinning (5 min, 2460 ***g***, 4°C) and removal of residual medium the pellet was dried for 60 min at room temperature. 300 µl of urea buffer was added [50 mM HEPES pH 7.4; 8 M urea; 2% SDS; cOmplete™ protease inhibitor cocktail (Roche, Basel, Switzerland); 10 mM PMSF; 10 mM ABA, 100 µg/ml leupeptin and 100 µg/ml pepstatin (all Sigma-Aldrich, St Louis, MO, USA)], and resuspended. For monitoring protein phosphorylation, NEB lysis buffer [50 mM HEPES pH 7.5, 100 mM NaCl, 2 mM DTT, 1% Triton™ X-100, 1 mM $MnCl_2$; cOmplete™ protease inhibitor cocktail and phosphatase inhibitor cocktail 3 (except for the λPPase sample)] was used. Cells were homogenized by beating (5×45 s, 4000 rpm) with glass beads (0.32-0.43 mm) in a BeadBug microtube homogenizer (Benchmark Scientific, Edison, NJ, USA). For dephosphorylation, the reaction mixture was then supplemented with 400 units of λPPase (NEB), and the reaction was allowed to proceed for 30 min at 30°C according to the manufacturer's instructions. Samples were diluted with respective buffers [based on Pierce™ BCA protein assay (Thermo Fisher Scientific) or direct protein concentration measurement using a NanoDrop™ ND-1000 Spectrophotometer for the phosphorylation study], mixed with 5× Laemmli protein sample buffer (312.5 mM Tris-HCl pH 6.8, 10% SDS, 25% glycerin, 25% β-mercaptoethanol and 0.2% Bromophenol Blue) and heated at 95°C for 5 min. Proteins were resolved using a 12.5% SDS-polyacrylamide gel or 6% 20 µM Zn(II) Phos-Tag™ SDS-polyacrylamide gel (40 µg of total protein in each sample) and wet-transferred to an Immobilon-E PVDF membrane (0.45 µm pore, Merck Millipore, Burlington, MA, USA).

The membrane was blocked with 5% milk (Serva Electrophoresis, Heidelberg, Germany) in TBST buffer (50 mM Tris-HCl pH 7.4 150 mM NaCl and 0.05% Tween 20) for 60 min, and incubated for 4 h at room temperature in 1% milk in TBST buffer with primary antibodies. To detect Lsp1–GFP, a mixture of anti-GFP mouse monoclonal conjugated with horseradish peroxidase (HRP; 1:1000, cat. no. sc-9996, Santa Cruz Biotechnology, Dallas, TX, USA) and anti-tubulin (YL1/2) rat monoclonal (1:10,000, ab6160, Abcam, Cambridge, UK; loading control) was used. After washing, the membrane was imaged for anti-GFP signal and subsequently incubated for 60 min at room temperature in 1% milk in TBST buffer with secondary antibody: for tubulin, anti-rat-IgG (goat, 1:10,000, Jackson ImmunoResearch, West Grove, PA, USA); for Lsp1–GFP, none. HRP chemiluminescence was monitored with Azure c400 (Azure Biosystems, Dublin, CA, USA) and VWR® Imager CHEMI Premium (VWR International, Radnor, PA, USA) detection system and analyzed using Image Studio Lite Ver 5.2 and VWR® Image Capture Software.

Spotting assay

Sensitivity to a range of stresses was evaluated using a solid medium assay. All strains were grown overnight in a rich YPD medium at 28°C, then diluted to equivalent concentrations of am optical density at 600 nm (OD_{600})=0.5 in water, and 10 µl of a 3-fold dilution series were spotted with a replica plater (R2383, Merck) onto YPD agar plates (2% agar, 2% peptone, 1% yeast extract, 2% glucose) with or without these chemicals: NaCl (1 M), myriocin (0.25 ug/ml or 0.5 ug/ml). Cells were grown on plates for 2–3 days at 28°C or 37°C, imaged with a Canon CanoScan 5600F scanner and growth differences were evaluated.

RNA isolation and NGS

Indicated strains were cultivated in 10 ml of SC medium for 24 h, pelleted (2460 ***g*** for 4 min, 4°C) and washed with 10 mM NaF/NaN_3. The supernatant was aspirated and the cells were homogenized by beating (5×30 s, 4000 rpm) with glass beads (0.32–0.43 mm) in 600 µl RLT buffer (RNeasy® kit, Qiagen) in a BeadBug microtube homogenizer (Benchmark Scientific, Edison, NJ, USA) and pelleted (610 ***g*** for 1 min). The supernatant was replaced into a fresh tube and treated with 10 µl proteinase K (Thermo Fisher Scientific) for 10 min at room temperature. Total RNA was isolated using the RNeasy® Plus Mini Kit (includes gDNA removal columns) followed by DNA digestion with a DNase Max® Kit (both Qiagen), according to the manufacturer's protocols. Samples were frozen in liquid nitrogen and delivered to the sequencing facility. RNA quality number (RQN, Agilent Fragment Analyzer 5200) of all samples was greater than 8. Sequencing libraries were prepared using polyA selection and sequenced using Illumina NextSeq 500.

Sequencing data were analyzed in R Studio. Quality of sequencing was verified using FastQC, rRNA and tRNA removed using SortMeRNA (Kopylova et al., 2012), and reads aligned to S288C genome reference (version R64-3-1_20210421; *Saccharomyces* genome database) using GSNAP (Wu and Nacu, 2010). Differential gene expression was analyzed using the DESeq2 package (Love et al., 2014), including normalization (median of ratios method) and log fold change (LFC) shrinkage (Stephens, 2017), with the significance cut-off adjusted *P*-values (corresponding to false discovery rate)<0.05 and LFC ($|\log_2 \text{FoldChange}| > 1$). Data visualization was performed using the ggplot2 package (Wickham, 2016). For exploratory analysis (PCA, GSEA and hierarchical clustering), normalized sequencing counts were further rlog2 transformed.

Microscopy image processing and data analysis

Image processing and analysis were performed in Fiji (ImageJ 1.53c) using custom-written macros, available at https://github.com/jakubzahumensky/Nce102_SL_paper (Zahumenský et al., 2022) and https://github.com/jakubzahumensky/Isc1_paper (Balazova et al., 2022) and cell segmentation masks made using the Cellpose software (Stringer et al., 2021), as described previously (Zahumenský et al., 2022). Statistical analysis was performed in GraphPad Prism 9 software. Statistical significance was determined by two-way ANOVA with Dunnett post test. Data distribution was assumed to be normal, but this was not formally tested.

Acknowledgements

NGS was performed at the Sequencing facility of IMG CAS on a commercial basis. Analysis of NGS data was greatly facilitated by R scripts and RMarkdown

documents previously developed by Jiří Novotný from IMG CAS. Special thanks belong to Satyendra Mondal who isolated the yeast RNA used for NGS analysis.

Competing interests
The authors declare no competing or financial interests.

Author contributions
Conceptualization: P.V., J.Z., J.M.; Methodology: P.V., J.Z., J.M.; Software: J.Z.; Validation: J.Z., J.M.; Formal analysis: J.Z.; Investigation: P.V., J.Z.; Resources: P.V., J.Z., J.M.; Data curation: J.Z.; Writing - original draft: P.V., J.Z., J.M.; Writing - review & editing: P.V., J.Z., J.M.; Visualization: P.V., J.Z.; Supervision: J.M.; Project administration: J.M.; Funding acquisition: J.M.

Funding
The work was supported by the Czech Science Foundation (Grantová Agentura České Republiky) project [grant number 20-04987S].

Data availability
Raw sequencing data, as well as normalized gene expression counts, from RNA-Seq have been deposited at GEO under accession number GSE211649 and are available at that URL. Genes differentially expressed in eg1Δnce102Δpil1Δ relative to the wild type are listed in Table S3.

Peer review history
The peer review history is available online at https://journals.biologists.com/jcs/lookup/doi/10.1242/jcs.260554.reviewer-comments.pdf

References
Appadurai, D., Gay, L., Moharir, A., Lang, M. J., Duncan, M. C., Schmidt, O., Teis, D., Vu, T. N., Silva, M., Jorgensen, E. M. et al. (2020). Plasma membrane tension regulates eisosome structure and function. *Mol. Biol. Cell* **31**, 287-303. doi:10.1091/mbc.E19-04-0218

Aresta-Branco, F., Cordeiro, A. M., Marinho, H. S., Cyrne, L., Antunes, F. and De Almeida, R. F. M. (2011). Gel domains in the plasma membrane of Saccharomyces cerevisiae. *J. Biol. Chem.* **286**, 5043-5054. doi:10.1074/jbc.M110.154435

Athanasopoulos, A., Gournas, C., Amillis, S. and Sophianopoulou, V. (2015). Characterization of AnNce102 and its role in eisosome stability and sphingolipid biosynthesis. *Sci. Rep.* **5**, 15200. doi:10.1038/srep15200

Balazova, M., Vesela, P., Babelova, L., Durisova, I., Kanovicova, P., Zahumensky, J. and Malinsky, J. (2022). Two different phospholipases C, Isc1 and Pgc1, cooperate to regulate mitochondrial function. *Microbiol. Spectr.* **10**, e0248922. doi:10.1128/spectrum.02489-22

Baxter, B. K., Didone, L., Ogu, D., Schor, S. and Krysan, D. J. (2011). Identification, in vitro activity and mode of action of phosphoinositide-dependent-1 kinase inhibitors as antifungal molecules. *ACS Chem. Biol.* **6**, 502-510. doi:10.1021/cb100399x

Berchtold, D., Piccolis, M., Chiaruttini, N., Riezman, I., Riezman, H., Roux, A., Walther, T. C. and Loewith, R. (2012). Plasma membrane stress induces relocalization of Slm proteins and activation of TORC2 to promote sphingolipid synthesis. *Nat. Cell Biol.* **14**, 542-547. doi:10.1038/ncb2480

Bermejo, C., Rodríguez, E., García, R., Rodríguez-Peña, J. M., Rodríguez De La Concepción, M. L., Rivas, C., Arias, P., Nombela, C., Posas, F. and Arroyo, J. (2008). The sequential activation of the yeast HOG and SLT2 pathways is required for cell survival to cell wall stress. *Mol. Biol. Cell* **19**, 1113-1124. doi:10.1091/mbc.e07-08-0742

Boggs, J. M. (1987). Lipid intermolecular hydrogen bonding: influence on structural organization and membrane function. *Biochim. Biophys. Acta.* **906**, 353-404. doi:10.1016/0304-4157(87)90017-7

Busto, J. V., Elting, A., Haase, D., Spira, F., Kuhlman, J., Schäfer–Herte, M. and Wedlich–Söldner, R. (2018). Lateral plasma membrane compartmentalization links protein function and turnover. *EMBO J.* **37**, e99473. doi:10.15252/embj.201899473

Deng, C., Xiong, X. and Krutchinsky, A. N. (2009). Unifying fluorescence microscopy and mass spectrometry for studying protein complexes in cells. *Mol. Cell. Proteomics* **8**, 1413-1423. doi:10.1074/mcp.M800397-MCP200

Desrivières, S., Cooke, F. T., Parker, P. J. and Hall, M. N. (1998). MSS4, a phosphatidylinositol-4-phosphate 5-kinase required for organization of the actin cytoskeleton in Saccharomyces cerevisiae. *J. Biol. Chem.* **273**, 15787-15793. doi:10.1074/jbc.273.25.15787

Dickson, R. C., Nagiec, E. E., Skrzypek, M., Tillman, P., Wells, G. B. and Lester, R. L. (1997). Sphingolipids are potential heat stress signals in Saccharomyces. *J. Biol. Chem.* **272**, 30196-30200. doi:10.1074/jbc.272.48.30196

Dunayevich, P., Baltanás, R., Clemente, J. A., Couto, A., Sapochnik, D., Vasen, G. and Colman-Lerner, A. (2018). Heat-stress triggers MAPK crosstalk to turn on the hyperosmotic response pathway. *Sci. Rep.* **8**, 15168. doi:10.1038/s41598-018-33203-6

Dupont, S., Beney, L., Ritt, J. F., Lherminier, J. and Gervais, P. (2010). Lateral reorganization of plasma membrane is involved in the yeast resistance to severe dehydration. *Biochim. Biophys. Acta – Biomembr.* **1798**, 975-985. doi:10.1016/j.bbamem.2010.01.015

Fröhlich, F., Moreira, K., Aguilar, P. S., Hubner, N. C., Mann, M., Walter, P. and Walther, T. C. (2009). A genome-wide screen for genes affecting eisosomes reveals Nce102 function in sphingolipid signaling. *J. Cell Biol.* **185**, 1227-1242. doi:10.1083/jcb.200811081

Fröhlich, F., Christiano, R., Olson, D. K., Alcazar-Roman, A., Decamilli, P., Walther, T. C., Frohlich, F., Christiano, R., Olson, D. K. and Alcazar-Roman, A. (2014). A role for eisosomes in maintenance of plasma membrane phosphoinositide levels. *Mol. Biol. Cell* **25**, 2797-2806. doi:10.1091/mbc.e13-11-0639

García-Rodríguez, L. J., Valle, R., Durán, Á. and Roncero, C. (2005). Cell integrity signaling activation in response to hyperosmotic shock in yeast. *FEBS Lett.* **579**, 6186-6190. doi:10.1016/j.febslet.2005.10.001

Gournas, C., Prévost, M., Krammer, E. and André, B. (2016). Function and regulation of fungal amino acid transporters: insights from predicted structure. In *Yeast Membrane Transport* (ed. J. Ramos, H. Sychrová and M. Kschischo) pp. 69-106. Cham: Springer International Publishing.

Gournas, C., Saliba, E., Krammer, E.-M., Barthelemy, C., Prévost, M. and André, B. (2017). Transition of yeast Can1 transporter to the inward-facing state unveils an α-arrestin target sequence promoting its ubiquitylation and endocytosis. *Mol. Biol. Cell* **28**, 2819-2832. doi:10.1091/mbc.e17-02-0104

Gournas, C., Gkionis, S., Carquin, M., Twyffels, L., Tyteca, D. and André, B. (2018). Conformation-dependent partitioning of yeast nutrient transporters into starvation-protective membrane domains - supplement. *Proc. Natl. Acad. Sci. USA* **115**, E3145-E3154. doi:10.1073/pnas.1719462115

Grossmann, G., Opekarová, M., Malinsky, J., Weig-Meckl, I. and Tanner, W. (2007). Membrane potential governs lateral segregation of plasma membrane proteins and lipids in yeast. *EMBO J.* **26**, 1-8. doi:10.1038/sj.emboj.7601466

Grossmann, G., Malinsky, J., Stahlschmidt, W., Loibl, M., Weig-Meckl, I., Frommer, W. B., Opekarová, M. and Tanner, W. (2008). Plasma membrane microdomains regulate turnover of transport proteins in yeast. *J. Cell Biol.* **183**, 1075-1088. doi:10.1083/jcb.200806035

Grousl, T., Opekarová, M., Stradalova, V., Hasek, J. and Malinsky, J. (2015). Evolutionarily conserved 5′-3′ exoribonuclease Xrn1 accumulates at plasma membrane-associated eisosomes in post-diauxic yeast. *PLoS One* **10**, e0122770. doi:10.1371/journal.pone.0122770

Hearn, J. D., Lester, R. L. and Dickson, R. C. (2003). The uracil transporter Fur4p associates with lipid rafts. *J. Biol. Chem.* **278**, 3679-3686. doi:10.1074/jbc.M209170200

Heidler, S. A. and Radding, J. A. (1995). The AUR1 gene in Saccharomyces cerevisiae encodes dominant resistance to the antifungal agent aureobasidin A (LY295337). *Antimicrob. Agents Chemother.* **39**, 2765-2769. doi:10.1128/AAC.39.12.2765

Herman, P., Vecer, J., Opekarova, M., Vesela, P., Jancikova, I., Zahumensky, J. and Malinsky, J. (2015). Depolarization affects the lateral microdomain structure of yeast plasma membrane. *FEBS J.* **282**, 419-434. doi:10.1111/febs.13156

Huang, X., Liu, J. and Dickson, R. C. (2012). Down-regulating sphingolipid synthesis increases yeast lifespan. *PLoS Genet.* **8**, e1002493. doi:10.1371/journal.pgen.1002493

Jenkins, G. M., Richards, A., Wahl, T., Mao, C., Obeid, L. and Hannun, Y. (1997). Involvement of yeast sphingolipids in the heat stress response of Saccharomyces cerevisiae. *J. Biol. Chem.* **272**, 32566-32572. doi:10.1074/jbc.272.51.32566

Kabeche, R., Baldissard, S., Hammond, J., Howard, L. and Moseley, J. B. (2011). The filament-forming protein Pil1 assembles linear eisosomes in fission yeast. *Mol. Biol. Cell* **22**, 4059-4067. doi:10.1091/mbc.e11-07-0605

Kabeche, R., Roguev, A., Krogan, N. J. and Moseley, J. B. (2014). A Pil1-Sle1-Syj1-Tax4 functional pathway links eisosomes with PI(4,5)P2 regulation. *J. Cell Sci.* **127**, 1318-1326. doi:10.1242/jcs.143545

Kabeche, R., Madrid, M., Cansado, J. and Moseley, J. B. (2015). Eisosomes regulate phosphatidylinositol 4,5-bisphosphate (PI(4,5)P2) cortical clusters and mitogen-activated protein (MAP) kinase signaling upon osmotic stress. *J. Biol. Chem.* **290**, 25960-25973. doi:10.1074/jbc.M115.674192

Karotki, L., Huiskonen, J. T., Stefan, C. J., Ziółkowska, N. E., Roth, R., Surma, M. A., Krogan, N. J., Emr, S. D., Heuser, J., Grünewald, K. et al. (2011). Eisosome proteins assemble into a membrane scaffold. *J. Cell Biol.* **195**, 889-902. doi:10.1083/jcb.201104040

Kopylova, E., Noé, L. and Touzet, H. (2012). SortMeRNA: fast and accurate filtering of ribosomal RNAs in metatranscriptomic data. *Bioinformatics* **28**, 3211-3217. doi:10.1093/bioinformatics/bts611

Lee, J.-H. H., Heuser, J. E., Roth, R. and Goodenough, U. (2015). Eisosome ultrastructure and evolution in fungi, microalgae, and lichens - supplement. *Eukaryot. Cell* **14**, 1017-1042. doi:10.1128/EC.00106-15

Liu, J., Huang, X., Withers, B. R., Blalock, E., Liu, K. and Dickson, R. C. (2013). Reducing sphingolipid synthesis orchestrates global changes to extend yeast lifespan. *Aging Cell* **12**, 833-841. doi:10.1111/acel.12107

Loibl, M., Grossmann, G., Stradalova, V., Klingl, A., Rachel, R., Tanner, W., Malinsky, J. and Opekarová, M. (2010). C terminus of Nce102 determines the structure and function of microdomains in the Saccharomyces cerevisiae plasma membrane. *Eukaryot. Cell* **9**, 1184-1192. doi:10.1128/EC.00006-10

Love, M. I., Huber, W. and Anders, S. (2014). Moderated estimation of fold change and dispersion for RNA-seq data with DESeq2. *Genome Biol.* **15**, 550. doi:10.1186/gb-2014-15-1-r1

Luo, G., Gruhler, A., Liu, Y., Jensen, O. N. and Dickson, R. C. (2008). The sphingolipid long-chain base-Pkh1/2-Ypk1/2 signaling pathway regulates eisosome assembly and turnover. *J. Biol. Chem.* **283**, 10433-10444. doi:10.1074/jbc.M709972200

Malínská, K., Malínský, J., Opekarová, M. and Tanner, W. (2003). Visualization of Protein Compartmentation within the Plasma Membrane of Living Yeast Cells. *Mol. Biol. Cell* **14**, 4427-4436. doi:10.1091/mbc.e03-04-0221

Malinsky, J. and Opekarová, M. (2016). New insight into the roles of membrane microdomains in physiological activities of fungal cells. *Int. Rev. Cell Mol. Biol.* **325**, 119-180. doi:10.1016/bs.ircmb.2016.02.005

Malinsky, J., Opekarová, M. and Tanner, W. (2010). The lateral compartmentation of the yeast plasma membrane. *Yeast* **27**, 473-478. doi:10.1002/yea.1772

Manzanares-Estreder, S., Pascual-Ahuir, A. and Proft, M. (2017). Stress-activated degradation of sphingolipids regulates mitochondrial function and cell death in yeast. *Oxid Med. Cell Longev.* **2017**, 2708345. doi:10.1155/2017/2708345

Mascaraque, V., Hernáez, M. L., Jiménez-Sánchez, M., Hansen, R., Gil, C., Martín, H., Cid, V. J. and Molina, M. (2013). Phosphoproteomic analysis of protein kinase C signaling in saccharomyces cerevisiae reveals Slt2 mitogen-activated protein kinase (MAPK)-dependent phosphorylation of eisosome core components. *Mol. Cell. Proteomics* **12**, 557-574. doi:10.1074/mcp.M112.020438

Miyake, Y., Kozutsumi, Y., Nakamura, S., Fujita, T. and Kawasaki, T. (1995). Serine palmitoyltransferase is the primary target of a sphingosine-like immunosuppressant, ISP-1/myriocin. *Biochem. Biophys. Res. Commun.* **211**, 396-403. doi:10.1006/bbrc.1995.1827

Moreira, K. E., Schuck, S., Schrul, B., Fröhlich, F., Moseley, J. B., Walther, T. C. and Walter, P. (2012). Seg1 controls eisosome assembly and shape. *J. Cell Biol.* **198**, 405-420. doi:10.1083/jcb.201202097

Nagiec, M. M., Nagiec, E. E., Baltisberger, J. A., Wells, G. B., Lester, R. L. and Dickson, R. C. (1997). Sphingolipid synthesis as a target for antifungal drugs. *J. Biol. Chem.* **272**, 9809-9817. doi:10.1074/jbc.272.15.9809

Olivera-Couto, A., Grana, M., Harispe, L. and Aguilar, P. S. (2011). The eisosome core is composed of BAR domain proteins. *Mol. Biol. Cell* **22**, 2360-2372. doi:10.1091/mbc.e10-12-1021

Pimentel, F. S. A., Machado, C. M., De-Souza, E. A., Fernandes, C. M., De-Queiroz, A. L. F. V., Silva, G. F. S., Del Poeta, M., Montero-Lomeli, M. and Masuda, C. A. (2022). Sphingolipid depletion suppresses UPR activation and promotes galactose hypersensitivity in yeast models of classic galactosemia. *Biochim. Biophys. Acta - Mol. Basis Dis.* **1868**, 166389. doi:10.1016/j.bbadis.2022.166389

Riggi, M., Niewola-Staszkowska, K., Chiaruttini, N., Colom, A., Kusmider, B., Mercier, V., Soleimanpour, S., Stahl, M., Matile, S., Roux, A. et al. (2018). Decrease in plasma membrane tension triggers PtdIns(4,5)P 2 phase separation to inactivate TORC2. *Nat. Cell Biol.* **20**, 1043-1051. doi:10.1038/s41556-018-0150-z

Sakata, K., Hashii, K., Yoshizawa, K., Tahara, Y. O., Yae, K., Tsuda, R., Tanaka, N., Maeda, T., Miyata, M. and Tabuchi, M. (2022). Coordinated regulation of TORC2 signaling by MCC/eisosome–associated proteins, Pil1 and tetraspan membrane proteins during the stress response. *Mol. Microbiol.* **117**, 1227-1244. doi:10.1111/mmi.14903

Schaber, J., Adrover, M. À., Eriksson, E., Pelet, S., Petelenz-Kurdziel, E., Klein, D., Posas, F., Goksör, M., Peter, M., Hohmann, S. et al. (2010). Biophysical properties of Saccharomyces cerevisiae and their relationship with HOG pathway activation. *Eur. Biophys. J.* **39**, 1547-1556. doi:10.1007/s00249-010-0612-0

Schorling, S., Vallée, B., Barz, W. P., Riezman, H. and Oesterhelt, D. (2001). Lag1p and Lac1p are essential for the Acyl-CoA-dependent ceramide synthase reaction in saccharomyces cerevisae. *Mol. Biol. Cell* **12**, 3417-3427. doi:10.1091/mbc.12.11.3417

Seger, S., Rischatsch, R. and Philippsen, P. (2011). Formation and stability of eisosomes in the filamentous fungus Ashbya gossypii. *J. Cell Sci.* **124**, 1629-1634. doi:10.1242/jcs.082487

Simons, K. and Ikonen, E. (1997). Functional rafts in cell membranes. *Nature* **387**, 569-572. doi:10.1038/42408

Stephens, M. (2017). False discovery rates: a new deal. *Biostatistics* **18**, 275-294. doi:10.1093/biostatistics/kxw041

Stradalova, V., Stahlschmidt, W., Grossmann, G., Blazikova, M., Rachel, R., Tanner, W. and Malinsky, J. (2009). Furrow-like invaginations of the yeast plasma membrane correspond to membrane compartment of Can1. *J. Cell Sci.* **122**, 2887-2894. doi:10.1242/jcs.051227

Stringer, C., Wang, T., Michaelos, M. and Pachitariu, M. (2021). Cellpose: a generalist algorithm for cellular segmentation. *Nat. Methods* **18**, 100-106. doi:10.1038/s41592-020-01018-x

Suarez, A., Ueno, T., Huebner, R., Mccaffery, J. M. and Inoue, T. (2014). Bin/Amphiphysin/Rvs (BAR) family members bend membranes in cells. *Sci. Rep.* **4**, 4693. doi:10.1038/srep04693

Tanigawa, M., Kihara, A., Terashima, M., Takahara, T. and Maeda, T. (2012). Sphingolipids regulate the yeast high-osmolarity glycerol response pathway. *Mol. Cell. Biol.* **32**, 2861-2870. doi:10.1128/MCB.06111-11

Tatebayashi, K., Tanaka, K., Yang, H.-Y., Yamamoto, K., Matsushita, Y., Tomida, T., Imai, M. and Saito, H. (2007). Transmembrane mucins Hkr1 and Msb2 are putative osmosensors in the SHO1 branch of yeast HOG pathway. *EMBO J.* **26**, 3521-3533. doi:10.1038/sj.emboj.7601796

Tatebayashi, K., Yamamoto, K., Nagoya, M., Takayama, T., Nishimura, A., Sakurai, M., Momma, T. and Saito, H. (2015). Osmosensing and scaffolding functions of the oligomeric four-transmembrane domain osmosensor Sho1. *Nat. Commun.* **6**, 4-6. doi:10.1038/ncomms7975

Vallejo, M. C. and Mayinger, P. (2015). Delayed turnover of unphosphorylated Ssk1 during carbon stress activates the yeast Hog1 MAP kinase pathway. *PLoS One* **10**, 1-10. doi:10.1371/journal.pone.0137199

Vangelatos, I., Roumelioti, K., Gournas, C., Suarez, T., Scazzocchio, C. and Sophianopoulou, V. (2010). Eisosome organization in the filamentous AscomyceteAspergillus nidulans. *Eukaryot. Cell* **9**, 1441-1454. doi:10.1128/EC.00087-10

Vaskovicova, K., Stradalova, V., Efenberk, A., Opekarova, M. and Malinsky, J. (2015). Assembly of fission yeast eisosomes in the plasma membrane of budding yeast: import of foreign membrane microdomains. *Eur. J. Cell Biol.* **94**, 1-11. doi:10.1016/j.ejcb.2014.10.003

Vaškovičová, K., Awadová, T., Veselá, P., Balážová, M., Opekarová, M. and Malinsky, J. (2017). mRNA decay is regulated via sequestration of the conserved 5′-3′ exoribonuclease Xrn1 at eisosome in yeast. *Eur. J. Cell Biol.* **96**, 591-599. doi:10.1016/j.ejcb.2017.05.001

Vaskovicova, K., Vesela, P., Zahumensky, J., Folkova, D., Balazova, M. and Malinsky, J. (2020). Plasma membrane protein Nce102 modulates morphology and function of the yeast vacuole. *Biomolecules* **10**, 1476. doi:10.3390/biom10111476

Vecer, J., Vesela, P., Malinsky, J. and Herman, P. (2014). Sphingolipid levels crucially modulate lateral microdomain organization of plasma membrane in living yeast. *FEBS Lett.* **588**, 443-449. doi:10.1016/j.febslet.2013.11.038

Voynova, N. S., Mallela, S. K., Vazquez, H. M., Cerantola, V., Sonderegger, M., Knudsen, J., Ejsing, C. S. and Conzelmann, A. (2014). Characterization of yeast mutants lacking alkaline ceramidases YPC1 and YDC1. *FEMS Yeast Res.* **14**, 776-788. doi:10.1111/1567-1364.12169

Walther, T. C., Brickner, J. H., Aguilar, P. S., Bernales, S., Pantoja, C. and Walter, P. (2006). Eisosomes mark static sites of endocytosis. *Nature* **439**, 998-1003. doi:10.1038/nature04472

Walther, T. C., Aguilar, P. S., Fröhlich, F., Chu, F., Moreira, K., Burlingame, A. L. and Walter, P. (2007). Pkh-kinases control eisosome assembly and organization. *EMBO J.* **26**, 4946-4955. doi:10.1038/sj.emboj.7601933

Wickham, H. (2016). *ggplot2*, 2nd ed. (ed. R. Gentleman, K. Hornik and G. Parmigiani). Cham: Springer International Publishing.

Winkler, A., Arkind, C., Mattison, C. P., Burkholder, A., Knoche, K. and Ota, I. (2002). Heat stress activates the yeast high-osmolarity glycerol mitogen-activated protein kinase pathway, and protein tyrosine phosphatases are essential under heat stress. *Eukaryot. Cell* **1**, 163-173. doi:10.1128/EC.1.2.163-173.2002

Wu, T. D. and Nacu, S. (2010). Fast and SNP-tolerant detection of complex variants and splicing in short reads. *Bioinformatics* **26**, 873-881. doi:10.1093/bioinformatics/btq057

Yang, J. and Tavazoie, S. (2020). Regulatory and evolutionary adaptation of yeast to acute lethal ethanol stress. *PLoS One* **15**, e0239528. doi:10.1371/journal.pone.0239528

Young, M. E., Karpova, T. S., Brugger, B., Moschenross, D. M., Wang, G. K., Schneiter, R., Wieland, F. T. and Cooper, J. A. (2002). The Sur7p family defines novel cortical domains in Saccharomyces cerevisiae, affects sphingolipid metabolism, and is involved in sporulation. *Mol. Cell. Biol.* **22**, 927-934. doi:10.1128/MCB.22.3.927-934.2002

Zahumensky, J. and Malinsky, J. (2019). Role of MCC/Eisosome in fungal lipid homeostasis. *Biomolecules* **9**, 305. doi:10.3390/biom9080305

Zahumenský, J., Mota Fernandes, C., Veselá, P., Del Poeta, M., Konopka, J. B. and Malínský, J. (2022). Microdomain protein Nce102 is a local sensor of plasma membrane sphingolipid balance. *Microbiol. Spectr.* **10**, e0196122. doi:10.1128/spectrum.01961-22

Zanolari, B., Friant, S., Funato, K., Suetterlin, C., Stevenson, B. J. and Riezman, H. (2000). Sphingoid base synthesis requirement for endocytosis in Saccharomyces cerevisiae. *EMBO J.* **19**, 2824-2833. doi:10.1093/emboj/19.12.2824

Zhang, X., Lester, R. L. and Dickson, R. C. (2004). Pil1p and Lsp1p negatively regulate the 3-phosphoinositide-dependent protein kinase-like kinase Pkh1p and downstream signaling pathways Pkc1p and Ypk1p. *J. Biol. Chem.* **279**, 22030-22038. doi:10.1074/jbc.M400299200

Ziółkowska, N. E., Karotki, L., Rehman, M., Huiskonen, J. T. and Walther, T. C. (2011). Eisosome-driven plasma membrane organization is mediated by BAR domains. *Nat. Struct. Mol. Biol.* **18**, 854-856. doi:10.1038/nsmb.2080

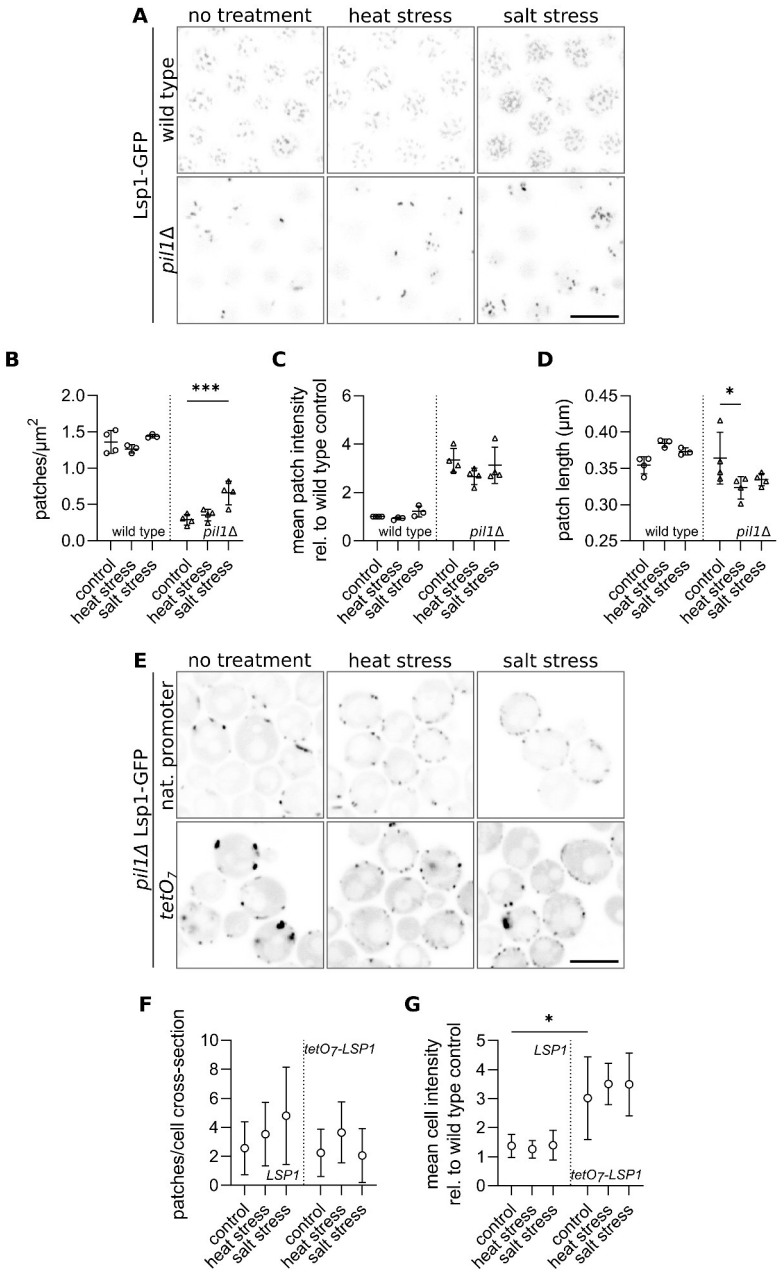

Fig. S1. Heat and salt stress induce the formation of Lsp1 foci in the plasma membrane. **A** Confocal fluorescence microscopy images (tangential sections) of *LSP1-GFP* expressing yeast cells grown exponentially for 4 hours at 28°C and subsequently shifted to 37°C for 2 hours or grown at 28°C in the presence of 1 M NaCl for 6 hours. Scale bar: 5 µm. **B-D** Quantification of the density of local Lsp1-GFP accumulations (patches)(B), mean patch intensity relative to the wild-type control (C) and patch length (D) in cells treated as in (A). Data are presented as mean ± SD from 4 biological replicates (circles – wild type, triangles – *pil1*Δ; 100–150 cells in each condition). **E** Confocal fluorescence microscopy images (transversal sections) of *pil1*Δ yeast cells expressing *LSP1-GFP* from either its native or *tetO7* promoter grown exponentially for 4 hours at 28°C and subsequently shifted to 37°C for 2 hours or grown at 28°C in the presence of 1 M NaCl for 6 hours. Scale bar: 5 µm. **F-G** Quantification of the number of local Lsp1-GFP accumulations (patches) per cell cross-section (F) and mean cell intensity relative to the wild-type control (G) in cells treated as in (E). Data are presented as mean ± SD from a single experiment (circles – wild type, triangles – *pil1*Δ; 100–150 cells in each condition). *tetO7-LSP1* indicates overexpression of *LSP1.* * – $P \leq 0.1$, *** – $P \leq 0.001$, two-way ANOVA.

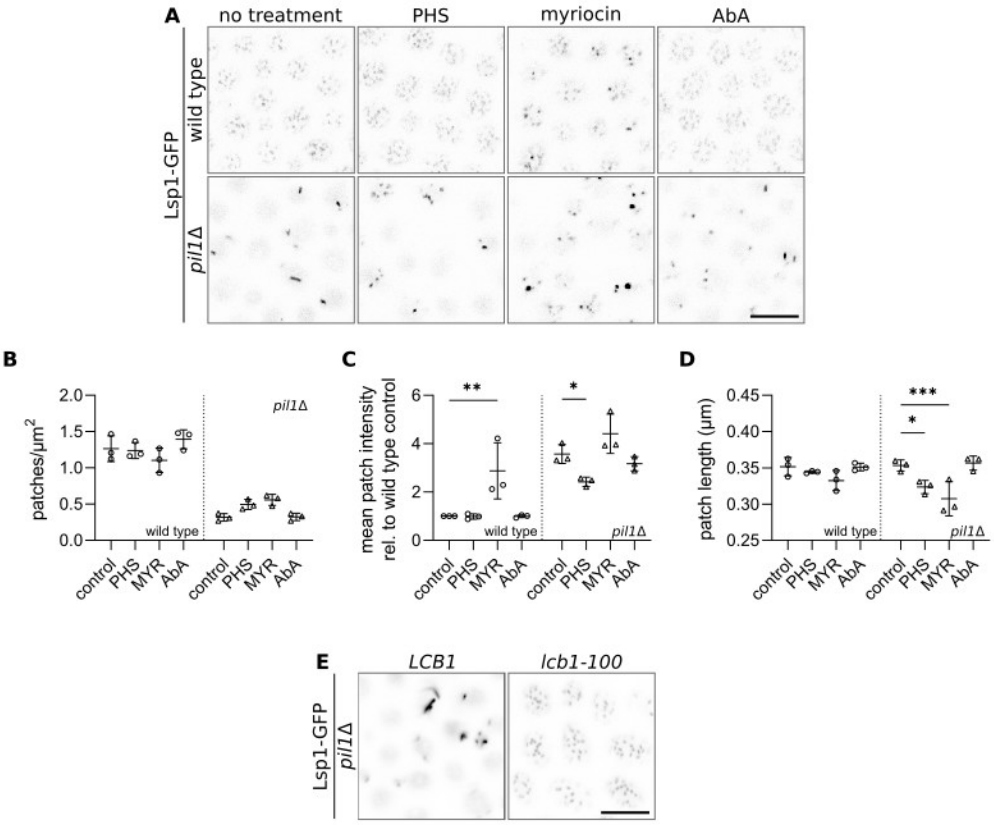

Fig. S2. Decrease in the activity of serine-palmitoyl transferase induces the formation of Lsp1 eisosomes in the plasma membrane; tangential sections.

A Confocal fluorescence microscopy images of *LSP1-GFP* expressing yeast cells (BY4742 background) grown exponentially for 4 hours at 28°C and treated with indicated chemicals for 2 hours. **B-D** Quantification of the density of local Lsp1-GFP accumulations (patches) (B), mean patch intensity relative to the wild-type control (C) and patch length (D) in cells treated as in (A). Data are presented as mean ± SD from 4 biological replicates (circles– wild type, triangles – pil1Δ; 150–200 cells in each condition). * – P ≤ 0.1, ** – P ≤ 0.01, *** – P ≤ 0.001, two-way ANOVA. E Confocal fluorescence microscopy images of LSP1-GFP expressing yeast cells (RH1800 background) grown exponentially for 5 hours at 25°C. PHS – phytosphingosine, 10 μM; MYR – myriocin, 10 μM; AbA –aureobasidin A, 1 μg/ml. Scale bars: 5 μm.

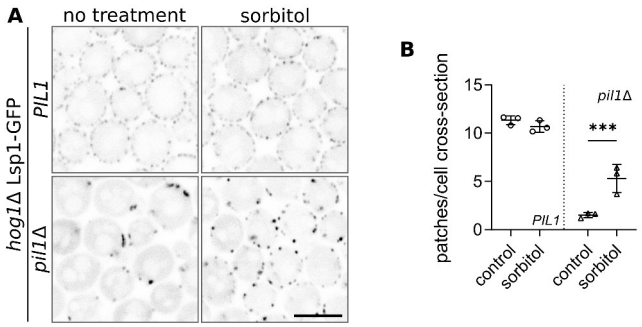

Fig. S3. Hog1 kinase is not required for Lsp1 eisosome formation in response to hyperosmotic stress
A Confocal fluorescence microscopy images (transversal sections) of *LSP1-GFP* expressing *hog1*Δ yeast cells grown exponentially for 6 hours at 28°C and treated with nothing or 1 M sorbitol for 25 minutes. Scale bar: 5 µm. **B** Quantification of the number of local Lsp1-GFP accumulations (patches) per cell cross-section in cells treated as in (E). Data are presented as mean ± SD from 3 biological replicates (circles – *hog1*Δ, triangles – *hog1*Δ*pil1*Δ; 170–230 cells in each condition). *** – $P \leq 0.001$, two-way ANOVA.

Table S1. Yeast strains used in the study.

Strain	Genotype	Source
BY4742, wild type	*MATα his3Δ1 leu2Δ0 lys2Δ0 ura3Δ0*	*Euroscarf*
hog1Δ	BY4742; *hog1::kanMX4*	*Euroscarf*
nce102Δ	BY4742; *nce102::kanMX4*	*Euroscarf*
pil1Δ	BY4742; *pil1::kanMX4*	*Euroscarf*
pil1Δa	BY4741; *pil1::kanMX4*	*Euroscarf*
seg1Δ	BY4742; *seg1::kanMX4*	*Euroscarf*
nce102Δ pil1Δ	*BY4742 except MET15; pil1Δ nce102Δ*	This study
seg1Δ pil1Δ	*BY4742 except MET15; seg1Δ pil1Δ*	Vaskovicova et al., 2015
lsp1Δ pil1Δ	*BY4742; lsp1Δ pil1Δ*	This study
seg1Δ nce102Δ	*BY4742 except LYS2 met15Δ0; seg1Δ nce102Δ*	This study
seg1Δ nce102Δ pil1Δ	*BY4742 except MET15; seg1Δ nce102Δ seg1Δ*	This study
Y114	*pil1Δ nce102Δ*; *LSP1::GFP::LEU2* (YIp128)	This study
Y172	BY4742; *LSP1::GFP::LEU2* (YIp128)	Zahumensky et al., 2022
Y257	*pil1Δ*; *LSP1::GFP::LEU2* (YIp128)	This study
Y430	*seg1Δ pil1Δ*; *LSP1::GFP::LEU2* (YIp128)	This study
Y1199	BY4742; *LSP1::GFP::HIS3* (pKT128)	This study
Y1214	Y1199*; LSP1::GFP::G418* (pCM225)	This study
Y1219	Y1214*; pil1::pFA6a-natMX6*	This study
Y1313	*lsp1Δ pil1Δ*; *SEG1::GFP::LEU2* (YIp128)	This study
Y1315	*nce102Δ*; *LSP1::GFP::LEU2* (YIp128)	This study
Y1377	*seg1Δ*; *LSP1::GFP::LEU2* (YIp128)	This study
Y1393	*seg1Δ nce102Δ pil1Δ*; *LSP1::GFP::LEU2* (YIp128)	This study
Y1395	*seg1Δ nce102Δ*; *LSP1::GFP::LEU2* (YIp128)	This study
Y1417	*hog1Δ*; *LSP1::GFP::LEU2* (YIp128)	This study
Y1421	Y1417; *pil1::pFA6a-natMX6*	This study
RH1800, wild type	*MATα leu2Δ0 trp1Δ0 ura3Δ0 lys2Δ0 bar1-1*	H. Riezman
lcb1-100	RH1800; *lcb1-100*	H. Riezman
Y1233	RH1800; *LSP1::GFP::LEU2* (YIp128)	This study
Y1234	*lcb1-100*; *LSP1::GFP::LEU2* (YIp128)	This study
Y1238	Y1233; *pil1::pFA6a-natMX6*	This study
Y1239	Y1234; *pil1::pFA6a-natMX6*	This study

Table S2. Parent strains used for the construction of double and triple-deletion strains

final strain	***MATα strain***	***MATα strain***
lsp1Δpil1Δ	*pil1Δ LSP1::mRFP::LEU2*	*lsp1Δ PIL1::GFP::URA3*
seg1Δpil1Δ	*pil1Δ SEG1::GFP::LEU2*	*seg1Δ PIL1::mRFP::URA3*
nce102Δpil1Δ	*pil1Δ NCE102::mRFP::URA3*	*nce102Δ PIL1::GFP::LEU2*
seg1Δnce102Δ	*nce102Δ SEG1::GFP::URA3*	*seg1Δ NCE102::mRFP::LEU2*
seg1Δnce102Δpil1Δ	*pil1Δnce102Δ SEG1::GFP::LEU2*	*pil1Δseg1Δ NCE102::mRFP::URA3*

All listed strains were constructed in the course of this study; for details see Methods

Table S3. Differentially expressed genes in the *seg1Δnce102Δpil1Δ* mutant relative to the wild type. Yeast were cultured and processed as described in Methods. As significance thresholds, log 2 fold change (LFC) was set to 1, P-adjusted < 0.05.

Click here to download Table S3

Movie 1. Disintegration of eisosome remnants and formation of Lsp1 eisosomes following myriocin-induced inhibition of SPT

LSP1-GFP expressing yeast cells were grown exponentially for 4 hours at 28°C and treated with 10 µM myriocin at time t = 0 min. Z-stacks were recorded for 2 hours in 5 min increments. The obtained images were drift corrected and maximum intensity projections calculated in proprietary Zeiss ZEN software. Timestamp shows time following myriocin addition in HH:MM format. Scale bar: 5 µm.